CHEMICAL REVIEWS

Review

pubs.acs.org/CR

Light-Harvesting and Amplified Energy Transfer in Conjugated Polymer Nanoparticles

Yifei Jiang and Jason McNeill*

Department of Chemistry, Clemson University, Clemson, South Carolina 29634, United States

ABSTRACT: Conjugated polymer nanoparticles are a class of nanoparticles with many useful and interesting properties, including very high fluorescence brightness, excellent photostability, and sensing capabilities. They also exhibit interesting and potentially useful phenomena, such as highly efficient energy transfer, anomalous single particle blinking, and twinkling phenomena associated with polaron motion. As little as one dye molecule per nanoparticle can efficiently quench the fluorescence of hundreds of polymer chromophore units. Similarly, loss of a single electron can result in quenching of hundreds of chromophores. These phenomena and properties are dictated by the nature of interactions between chromophores in this dense, nanoscale multi-chromophoric system, and are characterized as amplified energy transfer or multiple energy transfer. In this review, we summarize the key aspects of conjugated polymer nanoparticles optical properties and phenomena, and discuss the current understanding of exciton dynamics in these and related systems. In particular, our current understanding and theoretical models for amplified or multiple energy transfer based on exciton theory and Förster resonance energy transfer are explored.

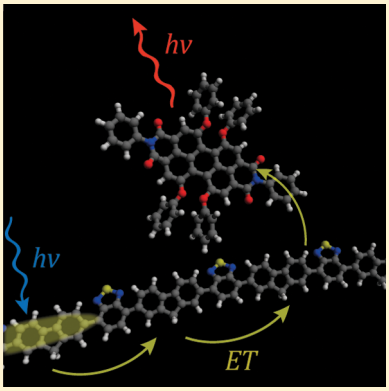

CONTENTS

1. Introduction A
2. Structure of CPNS B
3. Exciton in CPNS E
   3.1. Dimer Picture E
   3.2. Exciton Diffusion and Amplified Energy Transfer in CPNs F
   3.3. Exciton Quenching Processes I
4. Measurement of Exciton Transport in Dye-Doped CPNs I
   4.1. Steady-State Fluorescence of PFBT CPNs Doped with Perylene Red J
   4.2. Time Resolved Fluorescence of PFBT CPNs Doped with Perylene Red K
   4.3. Fluorescence Quenching in Undoped CPNs K
   4.4. Modeling of Quenching by Polarons L
5. Polaron Dynamics in CPNS M
   5.1. Fluorescence Saturation Behavior of CPNs N
   5.2. Reversible Fluorescence Decay Process of CPNs N
   5.3. Tracking Polaron Motion inside CPNs P
6. Conclusions R
Author Information R
   Corresponding Author R
   ORCID R
   Notes R
   Biographies R
Acknowledgments R
References R

1. INTRODUCTION

Conjugated polymers (CPs) have emerged as a class of technologically important materials due to their favorable combination of electrical and electro-optic properties as well as their flexibility and low-cost.[1−6] A wide variety of conjugated polymers have been synthesized, with bandgaps ranging from the UV to the near-infrared,[1,7,8] and with electron-conducting as well as hole-conducting properties.[9−12] While the bulk of conjugated polymer research has focused on thin films, conjugated polymer nanoparticles (CPNs) have emerged as a promising class of photoluminescent nanoparticles for a wide variety of applications, including as high-brightness fluorescent tags for nanoscale tracking and imaging,[13−17] and as chemical sensors[18−21] that function down to the single nanoparticle level.[22−24] CPNs (and related conjugated oligomer particles) are by most measures the brightest fluorescent nanoparticles demonstrated (roughly 20−100 times brighter than similar-sized colloidal semiconductor quantum dots under typical imaging conditions),[25,26] owing to the high extinction coefficient, high chromophore density, and (in some cases) high fluorescence quantum yield of the conjugated polymer. Photoswitching CPNs have also been demonstrated,[26−28] which could eventually lead to applications of CPNs to improve signal levels and resolution in photoswitching-based ultraresolution fluorescence imaging.[29,30] CPN sensors and photoswitches are typically doped with dyes that act as the sensors or photoswitches. Dye dopants are also used to red-shift the fluorescence of CPNs.[26,31,32] In addition to the

Special Issue: Light Harvesting

Received: June 30, 2016

 © XXXX American Chemical Society

DOI: 10.1021/acs.chemrev.6b00419
Chem. Rev. XXXX, XXX, XXX−XXX

imaging and sensing applications, there is also interest in layer-by-layer deposition of CPNs for fabrication of electro-optic devices with controlled nanostructure.[33−35] In CPNs containing a dopant dye, highly efficient energy transfer from the host polymer to the dopant dye is observed, indicating the presence of a multiple energy transfer or "amplified energy transfer" mechanism, in which the host polymer acts as a light-harvesting antenna that efficiently delivers energy to the dye.[26,31,36]

There is intense current interest in furthering our understanding of the processes that dictate CPN properties, particularly in understanding light-harvesting processes (i.e., processes associated with absorption of light, exciton dynamics, energy transfer, and various related processes) as well as using that understanding for tuning and improving CPN performance for various specific applications. As a nanoscale system with densely packed chromophores, CPNs can serve as a model synthetic light-harvesting system. Furthermore, CPNs can serve as a model system for understanding energy transport and even charge transport in conjugated polymer films and devices.[36,37] As such, this review is focused on recent results pertaining to the dynamics and processes associated with light harvesting and energy transport in CPNs, including excited electronic state dynamics, fast coherent energy transport, energy (exciton) diffusion, trapping, and energy transfer to dopant or defect species, or to other polymers in the case of blended CPNs. CPNs have also emerged as a promising model system for studying a variety of organic semiconductor device processes, such as charge transport,[37,38] charge separation in organic photovoltaics,[39] quenching of excitons by polarons,[40,41] and exciton diffusion or transport.[36,42] Additionally, a key process in the function of dye-doped or blended CPNs is energy transfer from the host conjugated polymer to the dopant.[26,31,36,43] Understanding the physical picture as well as the time scales and length scales of the various processes associated with energy transport is important for designing and optimizing nanoparticle fluorescence (and sensing and photoswitching) properties. We will outline current approaches to the experimental study and modeling of energy transfer and exciton transport in CPNs. Experimental results include steady-state and time-resolved fluorescence quenching studies, as well as single molecule studies. Modeling and theoretical efforts range from simple, empirical diffusion and energy transfer models to quantum-mechanical models. Finally, we will conclude with some perspectives on the current state of research in energy transfer, exciton transport and parasitic processes (e.g., trapping, quenching) in CPNs, and how the research informs a tentative comprehensive picture of excited state processes and energy transport in CPNs and related systems.

2. STRUCTURE OF CPNS

CPNs range in size between a few nanometers to microns, depending on preparation method, and they consist of somewhat closely packed chains of hydrophobic conjugated polymers, typically with a disordered or semicrystalline structure.[44−46] Suspended in water, or cast onto a surface from an aqueous suspension, the overall shape of the particle is typically governed primarily by interfacial tension and, thus, approximately spherical for smaller (<50 nm diameter) particles.[47] Here, we will focus our attention on smaller (<20 nm) nanoparticles. There is interest in knowing the detailed structure of CPNs, including polymer chain conformation and chain packing, largely motivated by the expectation (based on knowledge of other systems with similar chromophore density, such as organic semiconductors and light-harvesting complexes) that structure dictates the optical properties and related dynamics of CPNs. However, there are currently few experimental measurements or calculations providing detailed information about polymer conformational structure and chain packing in CPNs, though some molecular dynamics simulations[48] have started to appear in the literature. Additionally, some ultrafast and single molecule spectroscopy results provide some insight into the structure and the relationship between structure and optical properties and dynamics in CPNs and in single chains.[42,49−53] The gap in our knowledge of CPN structure and properties is (to some extent) filled by the vast literature on the relationship between structure and spectroscopy of organic semiconductor materials and conjugated polymers in solution and in thin films.[54−57] Other related dense multichromophoric systems, such as small molecule crystalline organic semiconductors and light-harvesting complexes, also have extensive literature.[58−60]

There is a complex set of factors that determine CPN structure. CPNs consist of one or a few (for <10 nm diameter particles) but often ten to hundreds of conjugated polymer chains. Assuming that CPNs are likely to share structural characteristics of similar systems, the structure of individual polymer chains in CPNs ought to resemble that of conjugated polymers or other "rigid rod" polymers in various solvents (Figure 1), ranging from a more or less extended structure,[61,62] to

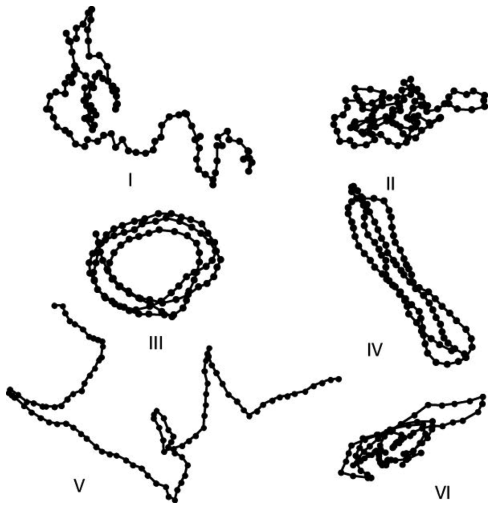

Figure 1. Typical conformations of a 100-segment homopolymer denoted as I, random coil; II, molten globule; III, toroid; IV, rod; V, defect-coil; and VI, defect-cylinder. Adapted with permission from ref 51. Copyright 2000 Macmillan Publisher Ltd.

a random coil,[63,64] molten globule,[65] collapsed chain,[66,67] or defect coil.[51] It is reasonable to expect that chain packing in CPNs, well way from the particle surface, should resemble the structure of thin films of the same or similar conjugated polymers, which ranges from amorphous[68,69] to semicrystalline[70−73] and crystalline,[74,75] depending on the backbone structure, side-chains, and heteroatoms that impart polarity. In terms of overall particle shape, one would expect CPNs to resemble latex particles of other hydrophobic polymers such as polystyrene particles, or perhaps they could resemble micelle shapes, which range from spherical to ellipsoidal and rod-like.

The conformation of conjugated polymer chains in solution is dictated by interactions between segments of the polymer chain, as well as solvent−chain interactions, the rigidity of the backbone

DOI: 10.1021/acs.chemrev.6b00419
Chem. Rev. XXXX, XXX, XXX−XXX

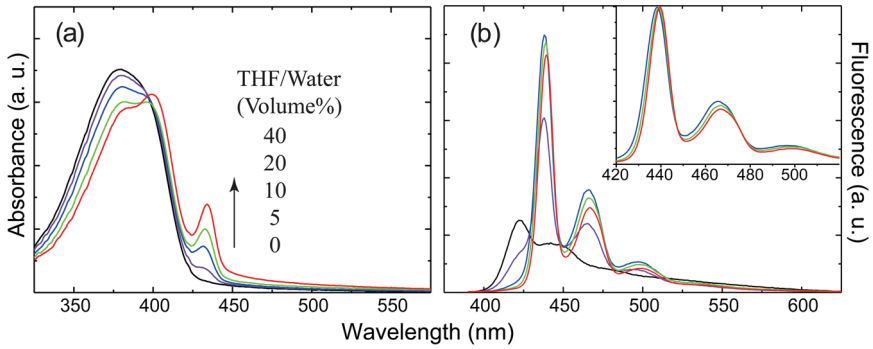

Figure 2. Absorption (a) and fluorescence spectra (b) of PFO nanoparticles with various fractions of β phase. As indicated by the arrow in part (a), the β phase absorption (435 nm) increases with the THF/water ratio. The inset indicates a slight red-shift in the fluorescence emission spectra with increasing β phase fractions. Adapted with permission from ref 44. Copyright 2008 American Chemical Society.

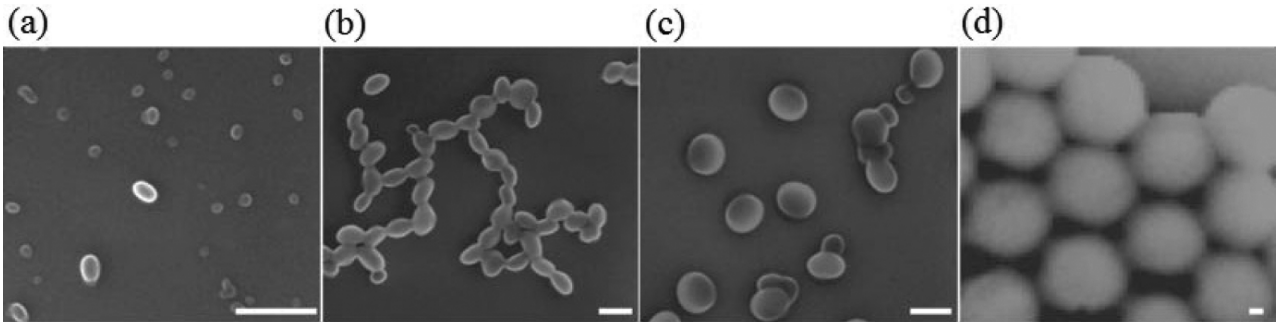

Figure 3. SEM images of nanoparticles of the conjugated polymer PFBT with different shapes and sizes. (a) 28 nm spheres with an aspect ratio of 1.0. (b) 140 nm long ellipsoids with an aspect ratio of 1.5. (c) 200 nm long ellipsoids with an aspect ratio of 1.2. (d) 1,000 nm spheres with an aspect ratio of 1.0. The white bar represents 200 nm in each plot. Adapted with permission from ref 47. Copyright 2005 Macmillan Publisher Ltd.

(i.e., the persistence length),[64,76] and side chain interactions.[77] Additionally, there is facile (thermally accessible) rotation about some bonds (e.g., the bond between the phenylene and vinylene moieties in poly(*p*-phenylenevinylene) and the phenylene–phenylene bond in polyphenylenes) in solution, which lead to at least temporary local deviations from the expected planar structure for sp^2-hybridized systems.[63,78] Furthermore, conformational defects (e.g., cis kinks and saturated (sp3) defects in PPVs), as well as chemical defects, can affect conformation in solution.[79] Solvent quality is another key determining factor in conjugated polymer conformation in solution; coil–globule transitions are likely to occur as a function of solvent quality.[80] In summary, the solution phase structure of isolated conjugated polymer chains is complex, depending on chain–solvent and chain–chain interactions, entropic effects (which can favor a disordered, random coil, or molten globule conformation), and the various degrees of freedom of the polymer. It is often the case that polymers that exhibit a more or less straight, planar conformation in thin films nevertheless adopt much more disordered conformations with somewhat twisted backbones in solution. There are some studies of polymer aggregate species in solution that show evidence of interchain interactions,[81] as in CPNs. This shows that in some cases structural characteristics or features present in the polymer in solution persist in the nanoparticle phase. It was previously reported that addition of organic solvent, for example THF or toluene, to an aqueous solution of poly(9,9-dioctylfluorene) (PFO) nanoparticles can induce the conformational transition from a glassy phase to a crystalline β phase, which persists in the CPNs even after evaporation of the organic solvent, similar to the solvent vapor annealing process observed in conjugated polymer films.[44] The fraction of the β phase depends on the amount of organic solvent added. The β phase in PFO CPNs is characterized by a narrow peak around 435 nm in the absorption spectrum and a red-shifted fluorescence spectrum with well-defined Franck–Condon progression (Figure 2). The red-shifted absorption spectrum of the β phase PFO compared to the glassy phase provides good overlap between the β phase absorption and the glassy phase emission spectra, which results in efficient energy transfer from the glassy phase to the β phase. PFO CPNs containing a β phase show higher quantum yield and longer fluorescence lifetime, which is likely a combined effect of efficient energy funneling to the β phase and reduced nonradiative pathways in the β phase compared to the glassy phase. This example shows how solvent quality controls the polymer conformation in CPNs and as a result dictates CPNs optical properties.

Some insight into conjugated polymer nanoparticle structure can be gleaned from electron microscopy studies of particle shape as a function of particle size and as a function of CP parameters, such as backbone structure and side chains. Terentjev et al. found that smaller CPNs (<30 nm dia.) prepared from in aqueous suspension from hydrophobic polymers using the miniemulsion technique exhibited spherical shape, as shown in Figure 3.[47] Meanwhile, for some liquid crystalline conjugated polymers, ellipsoidal shapes with aspect ratios up to 2:1 are observed for somewhat larger (100–300 nm dia.) particles. Larger, micron-sized particles are spherical. These results show the interplay between interfacial tension forces, which favor a spherical shape, and polymer rigidity and chain packing, which can favor a higher aspect ratio at some sizes. Very high aspect ratios can be achieved by self-assembly of conjugated polymers in

DOI: 10.1021/acs.chemrev.6b00419
Chem. Rev. XXXX, XXX, XXX–XXX

certain organic solvents or on substrates.[82−85] For example, poly(3-hexylthiophene) (P3HT) and other polythiophene (PT) derivatives can be assembled into a variety of nanostructures in toluene or chloroform, including nanorods, nanowires, nanorings, etc.[84,85] These structures are usually highly ordered and exhibit high carrier mobilities,[82,86] which makes them potentially useful in photovoltaics, supercapacitors, and transistor devices.

Single molecule fluorescence studies have provided useful information about conjugated polymer structure.[51,52,79,87−90] These studies typically involve single conjugated polymer chains dispersed in an inert polymer matrix, which are perhaps more indicative of conjugated polymer conformation in solution, as the polymer matrix acts as a "poor solvent", and thus could favor compact conformation. It is found that PPV based polymers with defects tend to form tetrahedral kinks in the polymer backbone and fold into cylinder conformation.[51] The ordering of the folded polymer structure, which typically ranges from semicrystalline to highly disordered, depends on the rigidity of the backbone and side chain interactions.[52,53] Some information about chain packing can be gleaned from single molecular spectra. Typically, in a highly ordered structure, excitons are further transferred to fewer and lower energy sites, which leads to red-shifted fluorescence spectra with clear vibronic structure.[53,91] A study of P3HT nanofibers assembled in toluene shows that the P3HT chains exhibit planar conformation with a long conjugation length, which gives rise to strong intrachain exciton coupling and J-aggregate type behavior.[84] By changing temperature and pressure to perturb the chain packing in P3HT nanofibers, the interchain interactions can be partially restored and H-aggregate character can be observed, which shows the delicate interplay between intrachain order and interchain interaction. While there is some evidence of crystalline domains in certain kinds of nanoparticles (Figure 4), for example CPNs made from P3HT or PFO,[44,46] many other CPNs appear to have highly disordered structure. Recently, tracking of individual charge carriers was reported in PFBT nanoparticles, and it was observed that the charge carriers were highly trapped with zero field mobilities ranging from 10^{-10} to 10^{-9} $cm^2/V\,s$,[37] which is consistent with a high degree of disorder in PFBT nanoparticles.

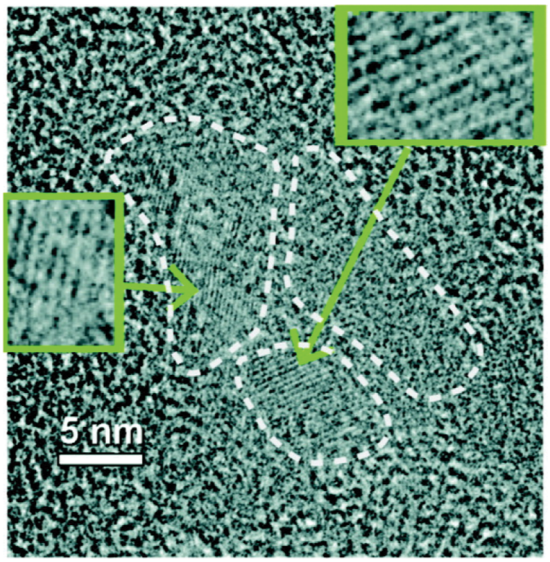

Figure 4. HRTEM image of a large P3HT particle (116 nm in diameter) with highlighted crystalline domains. Adapted with permission from ref 46. Copyright 2011 American Chemical Society.

The chemical environment of the polymer chains is another important factor in determining polymer conformation and can have profound effects on the properties. While the polymers employed in CPNs are typically hydrophobic, for CPNs in aqueous solution, there is water at the surface of the nanoparticle. Based on the rigidity of the polymer, some surface roughness is expected (for example, some chain segments likely project out beyond the particle surface), so it is likely that a significant fraction of the polymer interacts with water, particularly for smaller CPNs. Additionally, since the polymers could in some cases have a kinetically trapped conformation below the glass transition temperature, there may be pockets of trapped water in the particle interior. CPNs are often doped with dyes (including sensor dyes),[22,23,31] radical scavenger agent,[92] and various other species.[39,45] These affect the conformation of polymer chains and could increase permeability to ions, solvent, and other species present in solution. Furthermore, the distribution and orientation of dyes and other dopant species is another aspect of CPN structure that can affect optical properties and excited state properties. Gesquiere et al. reported the effect of PCBM (a fullerene derivative) doping on the bulk and single particle fluorescence spectra of nanoparticles of P3HT.[45] The presence of PCBM was observed to substantially quench the fluorescence of the polymer, as had been previously observed in PCBM-doped PT thin films. A slight blue-shift in the absorption spectra of the doped nanoparticles relative to the undoped nanoparticles was attributed to disruption of polymer chain packing by the fullerene. The fluorescence of single particles indicated a bimodal distribution, with some particles exhibiting a feature in the vicinity of 660 nm, while others exhibited a feature in the vicinity of 720 nm. Intriguingly, doping with PCBM appeared to increase the fraction of particles exhibiting ∼720 nm emission, perhaps indicating that the presence of PCBM increased the fraction of aggregate species with a red-shifted fluorescence. For dye-doped CPNs, energy transfer measurements yielded results that are consistent with a more or less random distribution of dyes.[31,36] There have also been attempts at controlling the distribution of various species comprising the CPN by controlled, sequential addition of various components during the particle formation process.[93,94] Fluorescence measurements of CPNs prepared using blends of two conjugated polymers indicate highly efficient energy transfer, suggesting a large area of contact between the two polymer species,[43,95] i.e., a more or less extended structure of the minority component rather than a segregated structure in which the minority component conformation is more like a close-packed sphere. This result also provides some indication that the majority component polymer chains also likely adopt a more or less extended conformation.

In summary, while there are some highly interesting and useful results appearing in the literature, we have much yet to learn about the detailed structure of CPNs. Additional experimental results and simulations are needed in order to better understand the subtle interplay of forces that determine CPN structure. Additional structural information will be needed in order to develop more accurate pictures of chromophore interactions and exciton dynamics in CPNs, as well as for designing CPNs with improved fluorescence brightness, photostability, and sensing or switching characteristics.

DOI: 10.1021/acs.chemrev.6b00419
Chem. Rev. XXXX, XXX, XXX−XXX

3. EXCITON IN CPNS

In this section, we will present the physical picture of Frenkel-type or molecular excitons, discuss some of the properties of excitons that are most relevant to energy (exciton) transport in CPNs, and discuss how CPN structure dictates exciton properties and dynamics relevant to energy transport. Molecular or Frenkel-type excitons are the principal neutral, electronically excited states of organic semiconductors that are involved in absorption and fluorescence in the UV and visible range. In dense, multichromophoric systems such as organic semiconductors and light-harvesting complexes, excitons are often described as shared or collective excitations that arise through the coupling of neighboring transition dipoles associated with the electronic transitions between the HOMO and LUMO states of π-conjugated chromophores. (In contrast, excitons in conventional inorganic semiconductors are typically Wannier-type excitons loosely characterized as a bound electron−hole pair.)

While conjugated polymers are organic semiconductors and share many characteristics with crystalline, small-molecule organic semiconductors such as anthracene or oligothiophene crystals,[58,96,97] there are important differences, due to disorder and polymer structure and consequent effects such as variability of conjugation length. For the sake of clarity, we will base our initial discussion on the Frenkel exciton model for crystalline, small molecule organic semiconductors, and then later discuss how excitons in CPNs differ from those of small molecule organic semiconductors. In conjugated polymer nanoparticles, there may be additional effects due to confinement or chain collapse, as well as effects due to nanoparticle composition (i.e., blended, composite, or doped CPNs).

3.1. Dimer Picture

Excitons exhibit spectroscopic features and phenomena that differ significantly from those of isolated chromophores. One phenomenon is red-shifted and blue-shifted absorption and emission spectra,[98−100] associated with the Davydov splitting.[101,102] Another phenomenon is changes in the radiative rate relative to the isolated chromophore.[98,99] Also, line-narrowing and changes in or loss of vibronic structure are often observed.[84,100,103] In the interest of providing an approximate physical picture and a framework for understanding these observations, it is useful to examine the dimer picture for excitons (Figure 5). The following description is intended to be tutorial rather than rigorous and definitive, and it should be accessible to those with some familiarity with quantum-mechanical perturbation theory. It is based loosely on the approach of Fleming et al.,[104] adapted to more closely resemble a typical derivation of two-state perturbation theory.[105] More rigorous approaches based on quantum field theory, taking into account more types of interactions, such as electron−phonon interactions, and that can provide quantitative predictions, can be found elsewhere.[58,97,106−110]

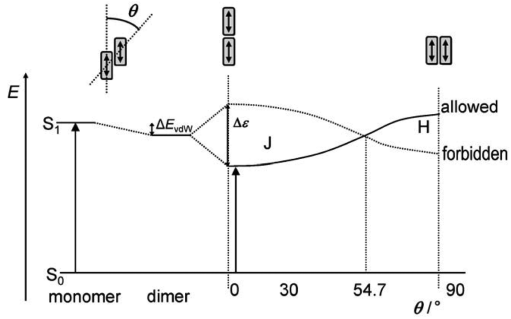

Figure 5. Energy diagram for parallel aligned dimers with various slip angles θ. Optical excitation from the ground state to the excited states depends on the slip angle θ. For $\theta < 54.78$ the lower energy excited state is allowed (J-band). For $\theta > 54.78$ the higher energy excited state is allowed (H-band). Adapted with permission from ref 100. Copyright 2011 Wiley-VCH.

Here, we assume two identical chromophores: a dimer (it is straightforward to extend the model to three or more identical chromophores). If our dimer picture consists of two identical chromophores at sites a and b, then we can denote an excitation at site a by the state $|a\rangle$, and an excitation at site b with $|b\rangle$. Following a degenerate two-state perturbation approach,[105] these are eigenstates of the unperturbed Hamiltonian, $\hat{H}_0$, such that $\hat{H}_0|a\rangle = \hbar\omega_0|a\rangle$ and $\hat{H}_0|b\rangle = \hbar\omega_0|b\rangle$. We then define a perturbation $\hat{V}$ representing the coupling between transition dipole moments at the two sites. We represent the coupling between the two sites as

$$\hat{V} = V_{ab}(|a\rangle\langle b| + |b\rangle\langle a|) \tag{1}$$

where V_{ab} contains any orientation and distance dependence and may be either negative or positive, depending on the orientations of the transition dipoles relative to the intermolecular axis, which is discussed in more detail below. It should also be noted that, for the case of three or more chromophores, the sign and magnitude of the coupling terms V_{ij} can vary for each pair of chromophores i and j, depending on their separation and relative orientation. The dimer states (solutions for the perturbed Hamiltonian) are then

$$|+\rangle = \frac{1}{\sqrt{2}}(|a\rangle + |b\rangle) \tag{2}$$

$$|-\rangle = \frac{1}{\sqrt{2}}(|a\rangle - |b\rangle) \tag{3}$$

where the states represent the transition dipoles oscillating either in-phase or out-of-phase, respectively. The corresponding energies are given by

$$E_{\pm} = \hbar\omega_0 \pm V_{ab} \tag{4}$$

For the dimer model, $2V_{ab}$ corresponds to the Davydov splitting or the exciton splitting.[101] A negative value for V_{ab} represents the case of transition dipoles oriented more or less parallel to the intermolecular axis, and systems with this behavior are referred to as J-aggregates. For J-aggregates, the $|+\rangle$ state is the lower energy state, and it represents the transition dipoles oscillating in-phase, with a head-to-tail orientation. For the case of dimers or aggregates oriented such that the transition dipoles are roughly perpendicular to the intermolecular axis (e.g., cofacial orientation), this corresponds to H-aggregates. For H-aggregates, V_{ab} is positive, and the out-of-phase $|-\rangle$ state is lower in energy.

Now let us consider the relative intensities of the various bands in terms of absorption and fluorescence. For the J-aggregate case, the overall net transition dipole moment of the lower-energy $|+\rangle$ state is higher than that of the isolated chromophore, whereas, for the higher-energy $|-\rangle$ state, the transition dipoles roughly cancel and the result is a much smaller (net) transition dipole moment for the state. Invoking Fermi's Golden Rule, the extinction coefficients and radiative rates are proportional to the (net) transition dipole moment squared, so the states with an increased net transition dipole moment have strong absorption features and reduced excited state lifetimes, resulting in the strong, red-

DOI: 10.1021/acs.chemrev.6b00419
Chem. Rev. XXXX, XXX, XXX−XXX

shifted absorption and fluorescence and superradiance (increased radiative rate) observed in the case of J-aggregates.[84,100] The coherent interaction between oscillating dipoles also results in narrowing of the absorption and emission features. Meanwhile, relaxation to the lowest energy exciton state and its lower overall transition dipole moment results in a typically low observed fluorescence quantum yield for H-aggregates.[73,111]

While the basic exciton picture outlined above gives delocalized states as solutions to the time-independent Schrödinger equation, we can use time-dependent perturbation theory in order to develop equations of motion for an excitation initially at $|a\rangle$ at $t = 0$. Using the conventional time-dependent perturbation theory approach, we obtain that the probability that the exciton is at $|b\rangle$ some later time is given by

$$P_b = \sin^2\left(\frac{V_{ab}t}{2\hbar}\right) \tag{5}$$

i.e., the system oscillates with a frequency of $V_{ab}/\hbar$. This system is closely related to that used to derive Fermi's Golden Rule.[112] Following that approach, we obtain

$$W = \frac{2\pi V_{ab}^2\rho}{\hbar} \tag{6}$$

where W is the (first-order) rate of exciton motion or transfer between coupled, equivalent sites, and ρ is the density of states.

The dimer picture is readily extended to larger systems containing three or more chromophores as well as 2D and 3D systems. In 3D crystalline solids, there are often one or two principal axes along which the transition dipole coupling is strongest, resulting in 2D exciton states with weaker coupling occurring between planes.[60] The effect of energetic disorder is to reduce the degree of coupling, and it can be approximated by switching to nondegenerate perturbation theory. The nondegenerate case results in energy splitting that is less than that of the degenerate case, with the difference between the site energies given by (approximately)

$$E_+ = \hbar\omega_a + \frac{V_{ab}^2}{\hbar\omega_a - \hbar\omega_b} \tag{7}$$

$$E_- = \hbar\omega_b - \frac{V_{ab}^2}{\hbar\omega_a - \hbar\omega_b} \tag{8}$$

where ω_a and ω_b are the frequencies for the unperturbed, nondegenerate chromophores, and we have assumed that a is the higher energy site. Clearly, for the nondegenerate case, the coupling of transition dipole moments has a reduced effect on the energy levels (i.e., reduced splitting) relative to the degenerate case. The wave functions are also less symmetric, and the exciton-type properties or effects (superradiance, etc.) are reduced. Toward the limit of weak coupling between transition dipoles, or for coupling that is much weaker than the difference in site energies, the system is better described using Förster energy transfer theory or another similar theory.[109,113] Thus, what emerges is a range of behavior with coherent, purely excitonic behavior at one end, characterized by a completely delocalized state and coherent oscillations of all transition dipole moments, and slower, shorter-range, incoherent Förster energy transfer governed by a rate equation with an inverse sixth-power distance-dependence at the other end. Typically, somewhat disordered collections of chromophores at noncryogenic temperatures fall somewhere in the middle of this range, and can be described as a mixed picture in which there is a range of exciton energies, with local regions described by localized excitons consisting of a few chromophores, exhibiting fast, partially coherent energy transport between chromophores, with some slower transport also occurring via weaker coupling described by an incoherent Förster mechanism. In this picture, lower-energy localized exciton states can act as "energy traps" or even quenching species (e.g., for H-aggregate-like states). A rough dividing line between the coherent exciton and Förster pictures can be declared at the point where either the thermal energy (k_BT) or energetic disorder is roughly equal to the transition dipole coupling strength. (That said, it should be noted that the term "exciton" is often applied broadly to the neutral electronic excited states in organic semiconductors and similar multichromophoric systems, and referring to a given excited state as an exciton does not necessarily imply a high degree of coupling, or coherent, collective excitation of a large number of chromophores.) For conjugated polymer films, red-shifted fluorescence spectra (relative to the polymer in solution) associated with J-type aggregation are most typically observed.[84,99] This result could simply be due to chromophore orientations more typically falling in the range that yields a J-type interaction, but in some cases it could be that more or less random orientations giving both J-type and H-type interactions, combined with the larger net transition dipole moment of J-type aggregates, as well as energy funneling to the lower-energy J-aggregate states, results in an overall red-shift.

For the case of CPNs, there are several characteristics that are different than the molecular crystal case and that can have profound effects on exciton properties and dynamics. For example, in aqueous suspensions, the electronic energy levels may also be affected by interactions with water molecules at the particle surface and water molecules that may be trapped in the particle interior. CPNs in some cases contain just a few chains, and those chains vary in molecular weight and conformation, and interchain interactions, which can lead to particle diversity. Variability in chain size and conformation can give rise to variations in conjugation length and thus variability in the energies, oscillator strengths, and orientation of the transition dipole moments of the chromophores. Additionally, the π molecular orbitals defining a given chromophore can change as the polymer conformation changes over time. Since excitons are comprised of these chromophore units, the energies of the chromophore HOMO and LUMO states, the state symmetries, and the distances and relative orientations of neighboring and nearby chromophores dictate the exciton energies and oscillator strengths. There may be particle size effects. The nature of these size effects is different than the case of other nanosized systems, such as quantum dots, and the effect of the overall system size on the energy levels and dynamics in CPNs is currently not well understood.

3.2. Exciton Diffusion and Amplified Energy Transfer in CPNs

Exciton diffusion is a key efficiency-determining step in polymer photovoltaic devices. For nanoparticle sensors and photoswitches based on conjugated polymers, exciton diffusion is also an important process.[20,21,26−28] Additionally, dye-doped CPNs have emerged as a model system for the study of exciton transport in conjugated polymers.[31,36] In addition to steady-state and time-resolved studies, single particle studies have emerged as a promising tool for elucidating the nature of exciton transport and energy processes in conjugated polymers, as well as a way to

DOI: 10.1021/acs.chemrev.6b00419
Chem. Rev. XXXX, XXX, XXX−XXX

determine how exciton transport and energy diffusion parameters are dictated by polymer structural characteristics as well as other factors, such as size effects, solvent interactions, blending with other conjugated polymers or inert polymers, and the addition of redox-active species. There is always a competition between exciton transport processes and other processes that result in trapping or quenching of excitons. Additionally, some exciton transport measurement methods involve exciton quenching (e.g., sensitized luminescence methods). While the underlying quantum-mechanical picture of energy transport is discussed above, here we will focus on empirical exciton transport pictures (i.e., exciton diffusion length) as well as various competing processes. Additionally, we will discuss how system dimensionality (i.e., 1D transport in rod-shaped particles or isolated polymer chains versus 3D transport in more spherical particles) affects exciton motion.

The basic quantum-mechanical description of exciton motion for a hypothetical, coherent exciton is discussed above. In disordered organic semiconductors such as conjugated polymers, exciton motion is often treated as an incoherent, stochastic, diffusion-like process, in which the basic picture is of a localized excitation on a single chromophore (or perhaps a somewhat localized exciton residing on a number of chromophores) transferring its energy to another, nearby equivalent chromophore or exciton site. Our discussion is primarily focused on singlet excitons, since most or all of the CPN experimental results are for singlet excitons and transport of triplet excitons in CPNs is still wholly or largely unexplored as of this writing. That said, the picture discussed here is based on general diffusive transport equations and is, to some degree, independent of the underlying transport mechanism and specific details of the excitons. In the conventional empirical exciton diffusion picture, the exciton equation of motion or diffusion-decay equation is

$$\frac{\partial n}{\partial t} = D\nabla^2 n - \frac{n}{\tau} \tag{9}$$

where n is the exciton density, D is the diffusion constant, and τ is the exciton lifetime. For steady-state diffusion from a point source, in the 1D case, the exciton density is given by[114]

$$n(x) = n_0 K_0\left(\frac{x}{L_D}\right) \tag{10}$$

where L_D is the exciton diffusion length and K_0 is the zero-order modified Bessel function of the second kind. L_D is a convenient figure of merit for comparing the exciton transport properties of various organic semiconductors.[59,115] and is related to the diffusion constant and the exciton lifetime by the expression

$$L_D = \sqrt{2ND\tau} \tag{11}$$

where N is the dimensionality of the system. For 2D, the exciton density is given by

$$n(R) = \frac{n_0 K_0(R/L_D)}{\sqrt{R}} \tag{12}$$

and for 3D, the expression is

$$n(R) = \frac{n_0 K_0(R/L_D)}{R} \tag{13}$$

For thin films, the exciton diffusion length can be experimentally determined by imaging of the exciton luminescence for a point-like excitation source and fitting eq 12.[116,117] However, since typical exciton diffusion lengths are on the order of 15 nm or less for conjugated polymers, imaging is complicated by diffraction issues. Waveguiding and other effects could also lead to significant errors. Sensitized luminescence is another common approach, in which the energy transfer to an acceptor dye followed by luminescence of the acceptor is used to obtain information about the exciton diffusion length. Including Förster-like energy transfer to a quencher into diffusion-decay expression yields

$$\frac{\partial n}{\partial t} = D\nabla^2 n - \frac{n}{\tau} - k_{et} n \tag{14}$$

where the energy transfer rate k_{et} is given by

$$k_{et} = \frac{1}{\tau}\left(\frac{R_0}{r}\right)^6 \tag{15}$$

where r is the exciton-quencher distance and R_0 is the Förster radius, which is typically on the order of a few nanometers for conventional organic dyes. The Förster radius depends on the spectral overlap between donor and acceptor, as well as the orientations of the transition dipoles.[118] While there are approximate analytical solutions to the above equations describing exciton diffusion and energy transfer, they usually assume an infinite system. Since conjugated polymer nanoparticles are finite, one approach is to model the time-dependent quantum mechanics of a small collection of chromophores, starting from a quantum-mechanical description similar to that outlined above.[119] Another approach is to use numerical approaches similar to those used in other diffusion and transport problems.[120] For example, one approach used to model exciton diffusion and energy transfer in CPNs doped with acceptor dyes, based on simulation of a random walk, which is used to model the effect of varying concentrations of dyes or quenching defects on the polymer (donor) fluorescence intensity and exciton lifetime, is described as follows.[31,36,43] A set of dye acceptor positions is randomly generated corresponding to the distribution of dyes within a (nanosized) sphere representing the nanoparticle. Random exciton positions are also generated, representing the distribution of excitons within the particle. At each time step Δt, each exciton is moved by a random amount along each axis, following a Gaussian distribution with

$$\sigma = \sqrt{2D\Delta t} \tag{16}$$

A check is performed at each time step to keep the excitons confined within the sphere. The rates of radiative decay, nonradiative decay, and energy transfer, as represented above, are used to determine the probability of each given exciton decaying during a given time step. Following a Monte Carlo kinetics approach, the probabilities are compared to random numbers to determine whether each exciton decays over a given interval. For each exciton lost to one of these processes, the fate is recorded in order to calculate the overall quenching efficiency (the fraction of excitons that decay via a quenching process). In addition, the exciton population is recorded at each time step, representing the exciton decay kinetics. In order to account for particle-to-particle variability in the spatial distribution of dyes, the random walk simulation is averaged over tens or hundreds of dye distributions. In some cases (such as for smaller nanoparticles), the Poisson distribution of quencher species must also be taken into account.

There are many variations on this approach. For example, instead of using Gaussian-distributed random numbers to

DOI: 10.1021/acs.chemrev.6b00419
Chem. Rev. XXXX, XXX, XXX−XXX

spatially propagate the excitons at each time step, the excitons can be confined to a grid with spacing Δx. For that case, the probability of an exciton to hop to a nearest-neighbor site within a given time interval Δt is given by

$$P_{hop} = 2D\frac{\Delta t}{\Delta x^2} \tag{17}$$

The grid spacing can either be set to a small value, in order to approximate the continuum transport equations above, or it can be set to the interchromophore spacing, to represent the physical picture of excitations hopping between chromophores. Another approach is to invoke the steady-state approximation as well as a grid approach, which gives rise to a system of equations that can be solved by matrix methods.[37]

Previously, we have reported quenching efficiencies and exciton lifetime distributions as a function of dopant concentration in dye-doped CPNs.[36] A more detailed discussion of the comparison between theory and experiment, including determination of the exciton diffusion length, is given later in this review, but one of the more salient observations is that both experimental results and exciton diffusion and energy transfer model calculations indicate that the combination of long-range Förster energy transfer and exciton diffusion results in highly efficient energy transfer overall, resulting in effective quenching volumes that are significantly higher than those obtained from either Förster transfer or exciton diffusion alone. This phenomenon is sometimes referred to as "amplified energy transfer" or "multiple energy transfer", in reference to the multiple energy transfer steps that can occur as a mobile exciton passes between chromophores of the organic semiconductor ("host" or "donor") prior to energy transfer to the dye ("acceptor"). A similar phenomenon, termed "superquenching", has been observed in conjugated polymer electrolytes.[18,121] This leads to the question of how to describe the amplification mathematically, such as in terms of an amplification factor. We are also interested in how various system parameters (e.g., exciton diffusion length, particle size) affect the degree of energy funneling or amplified energy transfer. There are several possible approaches for developing useful descriptions or experimental measures of amplified energy transfer. We will start by developing a mathematical expression for an amplification factor, based on the physical picture of exciton diffusion, and discuss some (possibly approximate) experimental measures. Our physical picture is an organic semiconductor and dopant system characterized by an exciton diffusion length L_D, an exciton lifetime τ_0, and a donor−acceptor Förster radius R_0. Let us further assume that the system is a nanoparticle of radius r_{np}, and that there is a single acceptor (quencher) in the center of the nanoparticle. We can define an amplification factor f_a,

$$f_a = \frac{q}{q_0} \tag{18}$$

where q is the quenching efficiency including both exciton diffusion effects and Förster effects, and q_0 is the (energy transfer) quenching efficiency in the absence of exciton diffusion. In the limit of large nanoparticle volume, the ratio of quenching efficiencies is equal to the ratio of quenching volumes,

$$f_a = \frac{V_q}{V_0} \tag{19}$$

where V_q is the quenching volume including exciton diffusion, and V_0 is the quenching volume assuming only Förster transfer. From this we obtain

$$f_a = \frac{R_q^3}{R_0^3} \tag{20}$$

where R_q is the quenching radius. If we relax the requirement of large nanoparticle volume, then R_q is an *effective* quenching distance. We can also define the effective quenching volume as

$$V_q = qV_{np} = \frac{4\pi q r_{np}^3}{3} \tag{21}$$

For a single quencher at the center of a particle of radius r_{np}, the spatially averaged quenching efficiency is obtained by integrating the quenching efficiency expression

$$q_0(r) = \frac{1}{1 + \left(\frac{r}{R_0}\right)^6} \tag{22}$$

yielding

$$q_0 = \frac{R_0^3}{r_{np}^3} \arctan \frac{r_{np}^3}{R_0^3} \tag{23}$$

Combining with the above expression for the quenching volume yields the following expression for the quenching volume of a single acceptor at the center of a particle, in the absence of exciton diffusion,

$$V_q = \frac{4\pi R_0^3}{3} \arctan \frac{r_{np}^3}{R_0^3} \tag{24}$$

In the large particle limit, the (diffusion-free) quenching volume is a factor of $\pi/2 \approx 1.57$ larger than that of a sphere of radius R_0, whereas, for $r_{np}/R_0 = 2$, the factor is 1.45. Based on these results, the effective quenching radius is roughly 16% larger than the Förster radius, in the large particle limit.

There is no closed form, analytical expression for the effective quenching volume for combined exciton diffusion and energy transfer. An interpolation formula has been developed for some similar cases involving a combination of energy transfer and diffusion in solution, but it has not been adapted to exciton diffusion.[122] Integrating numerically (using the random walk approach described above), the amplification factor for various particle sizes (r_{np} = 4, 8, 12 nm), R_0 = 3 nm, and various values of the diffusion length (L_D = 3, 6, 9, 12, 15 nm) were determined (Figure 6a). A reasonable exciton diffusion length of 15 nm results in f_a = 4.4, indicating that exciton diffusion increases the

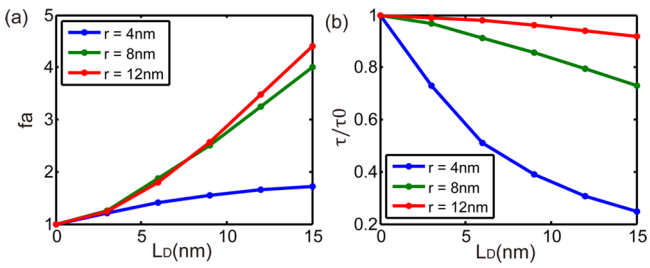

Figure 6. Simulation results for a single acceptor at the center of a nanoparticle: (a) amplification factor f_a, (b) normalized exciton lifetime τ/τ_0 for various exciton diffusion lengths L_D and three particle sizes.

DOI: 10.1021/acs.chemrev.6b00419
Chem. Rev. XXXX, XXX, XXX−XXX

effective quenching volume of the acceptor by this factor. This corresponds to a roughly 63% increase in the effective quenching radius. Even for a more modest diffusion length of 6 nm, diffusion nearly doubles the quenching volume. Of course, for smaller particles (or for the related case of high acceptor density), the quenching efficiency of a single acceptor is higher and the quenching volume is limited by the particle volume, so the effect of exciton diffusion is less pronounced—for nanoparticles with a radius of 4 nm, the amplification factor is less than 2. This reflects the fact that, if most excitons are within the quenching sphere, then a smaller fraction of excitons can be carried to the quenching sphere by diffusion. The exciton lifetimes or the associated energy transfer rates provide additional information (Figure 6b), particularly in the case of small particles, for which the effect of diffusion on exciton lifetimes is more pronounced than its effect on quenching efficiency. For r_{np} = 4 nm, the exciton lifetime decreases from close to τ_0 for L_D = 0 nm to less than $0.24\tau_0$ for L_D = 15 nm. While the results discussed here are for a single acceptor at the center of a nanoparticle, similar results are obtained for a random distributions of multiple acceptors, except that, for multiple quenchers, the overall quenching efficiency (per acceptor) is lower and the effect of diffusion is somewhat less pronounced, owing to overlapping quenching volumes. Summarizing, it is apparent that, for conjugated polymer nanoparticles, amplified energy transfer is a significant effect, with amplification factors ranging from roughly 2 to more than 4 over the expected range of exciton diffusion lengths. Additionally, exciton diffusion lengths are typically larger than Förster radius, often by a factor of 2 or more, indicating that there are often multiple donor−donor energy transfer steps. Furthermore, the effect of particle size on energy transfer efficiency in CPNs is complex. On the one hand, reducing particle size to less than the quenching sphere should result in increased energy transfer efficiency as well as the energy transfer rate. However, at a given weight fraction of acceptor dye (relative to the donor), the number of dyes per nanoparticle can fall well below unity, so that, overall, a population of nanoparticles would exhibit less energy transfer efficiency. In the limit of large particle size, it is expected that exciton quenching is well-described by a complex mixture of Förster transfer and diffusion-dependent (dynamic) quenching, similar to that observed in bulk crystals,[123,124] whereas, for smaller particles at low (fixed) doping levels, there is likely to be a higher quenching rate occurring in a smaller fraction of particles. In the limit of small particles (i.e., for particles with a radius that is a fraction of the quenching radius), those particles that contain a quencher should exhibit very fast, highly efficient energy transfer that is effectively or nearly indistinguishable from static quenching (i.e., most of the donor fluorescence is quenched in the fraction of particles that contain a quencher).

3.3. Exciton Quenching Processes

Like the fluorescent excited states of isolated molecules, excitons undergo relaxation by a number of pathways, including internal conversion, intersystem crossing, and radiative relaxation. There are also exciton quenching processes, some of which are analogous to quenching processes of fluorescent molecules in solution, such as intermolecular charge transfer. Additionally, the interactions between the densely packed chromophores in excitonic systems can have a significant impact on various quenching processes. Formation of various aggregate excited species that are nonfluorescent or weakly fluorescent can quench the luminescent ecited state in organic semiconductor materials. Such species include the aforementioned H- and J-aggregates as well as excimers and exciplexes. These species are sometimes loosely referred to collectively as aggregate species. Chemical defects can also quench luminescence. At high excitation intensities, exciton collisions can lead to loss of exciton population. In particular, buildup of relatively long-lived triplet exciton species (if either the triplet quantum yield is high or the excitation intensity is high) can result in substantial reduction in singlet luminescence.[125,126]

Excited state charge transfer (exciton dissociation) can lead to the formation of charge-carrying polarons. Hole polarons are π-conjugated radical cation species, and typically exhibit red-shifted absorption relative to the neutral polymer, which makes them good Förster energy transfer acceptors. Hole polarons are also often essentially nonfluorescent. Thus, hole polarons are likely to act as quenching acceptor species. Previously, it was assumed that luminescence quenching by polarons was negligible under typical electrically neutral conditions, primarily because the exciton dissociation energy is typically on the order of a few hundred millielectronvolts, so according to Boltzmann statistics fewer than 1 in 10,000 thermalized excitons are dissociated, loosely speaking. However, there are several factors that can lead to significant quenching by polarons. Including effects of multiple energy transfer, the polaron quenching radius is estimated at between 5 and 15 nm—sufficient to quench thousands (or more) chromophores, assuming a high chromophore packing density of roughly 1 chromophore per cubic nanometer. Indeed, quenching by a single hole polaron has been observed to cause significant blinking in single CP molecules and single small CPNs—as high as 90% quenching is observed in some cases.[37,40,41,127] Similar highly efficient quenching by hole polarons has been observed in conjugated polymer thin films.[128−130] Energetic disorder can also effectively lower the barrier to polaron formation, and disorder can result in trapping and stabilization of polarons, resulting in longer polaron lifetimes and thus a larger steady-state polaron density. Additionally, and perhaps more importantly, partial oxidation of the polymer can increase the polaron density. Doping of CPNs with reducing species or antioxidant species has been shown to increase the fluorescence quantum yield of CPNs, perhaps indicating that the reducing species suppress the buildup of polarons.[92] There is evidence (discussed in more detail below) that amplified quenching by hole polarons has significant effects on the measurement of exciton diffusion in CPNs (and likely in related systems such as conjugated polymer thin films and devices), in some cases reducing the apparent exciton diffusion length by a factor of 2, or perhaps more.

4. MEASUREMENT OF EXCITON TRANSPORT IN DYE-DOPED CPNS

The optical properties of CPNs are determined by the dynamics and transport processes of excitons. Thus, measurement of the dynamics and transport processes of excitons in CPNs is of interest, both due to the effect of such processes on CPN properties (particularly for CPNs doped with dyes acting as sensors, or for shifting fluorescence), and due to CPNs serving as a model system for aspects of exciton dynamics in bulk films. There are several competing approaches to measurement of exciton transport in organic semiconductor films and crystals, including sensitized luminescence of uniformly doped films and crystals,[123,124] luminescence of layered structures in which exciton diffusion from the semiconductor layer to an acceptor layer is measured via luminescence,[59] and near-field microscopy.[116] Here we consider how aspects of these various

DOI: 10.1021/acs.chemrev.6b00419
Chem. Rev. XXXX, XXX, XXX−XXX

approaches can be adapted to measure exciton transport parameters in CPNs. Steady-state and time-resolved measurements of quenching of the host polymer fluorescence are compared to model results to obtain an indirect measure of exciton transport parameters, such as the exciton diffusion length. There are several different and potentially useful or interesting aspects of CPN-based measurements of exciton diffusion as compared to more traditional thin-film approaches, including the following. There is control of particle size, which can be exploited to probe the effects of confinement on exciton transport. It is straightforward to prepare CPNs at various dye doping levels, so that experimental measurements over a range of doping levels can be readily compared to model results. For smaller CPNs, a single dye molecule per particle is sufficient to yield measurable and, in some cases, highly efficient energy transfer. The size of particles is similar to that of the length scales of heterogeneity of CPNs; thus, we can obtain information about the effects of nanoscale heterogeneity on transport. Single-particle measurements can be used to probe particle-to-particle heterogeneity and dynamic heterogeneity, and the time scales of dynamic heterogeneity can give clues about what processes are involved. It is straightforward to include other species that can represent exciton traps or charge carrier traps. The redox environment can be controlled by addition of redox-active molecular species.[92] Measurements of exciton transport and quenching behavior in CPNs containing a blend of two different conjugated polymers provide information about the physical picture of energy transfer in blended polymer systems, as well as the effects of polymer conformation.[43,95]

An important issue in the use of models to extract physical parameters is the accuracy of the underlying physical picture and its explicit or implicit assumptions. There are a number of implicit assumptions about the nature of excitons and the exciton transport process in the diffusion picture described above. For example, this picture assumes that transport is via a uniform diffusion-like process, whereas the actual system is granular and heterogeneous. Thus, a very good fit to the continuum diffusion model would provide some indication that the net effects of such heterogeneity on the exciton transport parameters are minor, whereas deviation from the model results could provide motivation to pursue more detailed (e.g., molecule-based) descriptions as well as providing key tests of such descriptions—from an applications perspective, a higher-level or finer-grained theoretical description is only successful to the extent that it provides an improved fit with experimental results (preferably with fewer adjustable parameters) and thus provides improved predictions that could thus be useful in the design of materials with improved properties. Additionally, there is often a trade-off in that while for simpler models the relationship between model parameters and measured values is usually straightforward, increasing the level of complexity of a model can obscure such relationships. Of course, we need not choose just one level of description, and often much can be learned from comparing the results of various models with varying levels of detail and approximation. Here we examine various issues regarding extracting exciton transport parameters in more detail.

4.1. Steady-State Fluorescence of PFBT CPNs Doped with Perylene Red

Recently, time-resolved fluorescence quenching results for dye-doped CPNs were reported for the first time (steady-state results for another system had been reported previously),[31] along with a comparison to the results of an exciton diffusion model.[36] The host conjugated polymer was poly[(9,9-dioctylfluorenyl-2,7-diyl)-*co*-(1,4-benzo-{2,1′,3}-thiadiazole)] (PFBT, MW 10,000, polydispersity 1.7), and the dye employed was perylene red (Figure 7a). The dye was chosen for its good Förster overlap with

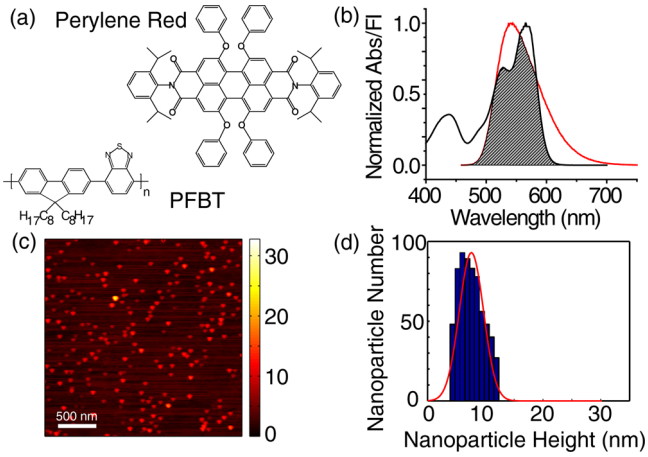

Figure 7. (a) Chemical structures of perylene red and PFBT. (b) Normalized perylene red absorption spectrum (black line) and PFBT fluorescence spectrum (red line) in THF. The spectral overlap is shown by the shaded area. (c) Representative AFM image of undoped PFBT CPNs. (d) Particle size histogram obtained from the AFM image shown in (c). Adapted with permission from ref 36. Copyright 2013 American Chemical Society.

the host polymer (Figure 7b). Nanoparticles 8 ± 2 nm in diameter were prepared by a nanoprecipitation method. The dye was incorporated by coprecipitation. The steady-state fluorescence measurements indicated highly efficient energy transfer from the polymer to the dye, suggesting the occurrence of multiple energy transfer, i.e., Förster energy transfer combined with exciton diffusion.

The host fluorescence intensity was used as a measure of the energy transfer quenching of the host polymer by the acceptor dye. Alternatively, the acceptor fluorescence can be used, but concentration quenching of the acceptor (dye aggregation) can introduce systematic error. Initial characterization of the quenching process can be obtained using a Stern−Volmer plot. While the Stern−Volmer equation is typically derived assuming either (a) free diffusion of quenching species in solution and collisional quenching (dynamic quenching) or (b) equilibrium binding of the quencher in solution to yield a nonfluorescent dimer (static quenching), the case of exciton diffusion is sufficiently similar mathematically to the case of quencher diffusion in solution that it is not surprising that the Stern−Volmer plot of F_0/F versus acceptor concentration is linear (Figure 8b), as expected for the conventional solution-phase Stern−Volmer mechanisms. Similarly, assuming static quenching within a certain quenching radius, for quencher species in a host matrix, yields Stern−Volmer-like behavior for F_0/F, similar to the case of static quenching in solution. In the present case, the physical interpretation of the Stern−Volmer constant, K_{sv}, is that it yields a measure of quenching efficiency of the acceptor dye. If the concentration is calculated in terms of a molecular ratio (molecules of quencher per molecules of host), then an (approximate) physical interpretation of the Stern−Volmer constant is (roughly) the number of host molecules quenched by a single quencher, on average. A linear fit yields K_{sv} = 37, indicating that roughly 37 molecules of PFBT (MW = 10000) are

DOI: 10.1021/acs.chemrev.6b00419
Chem. Rev. XXXX, XXX, XXX−XXX

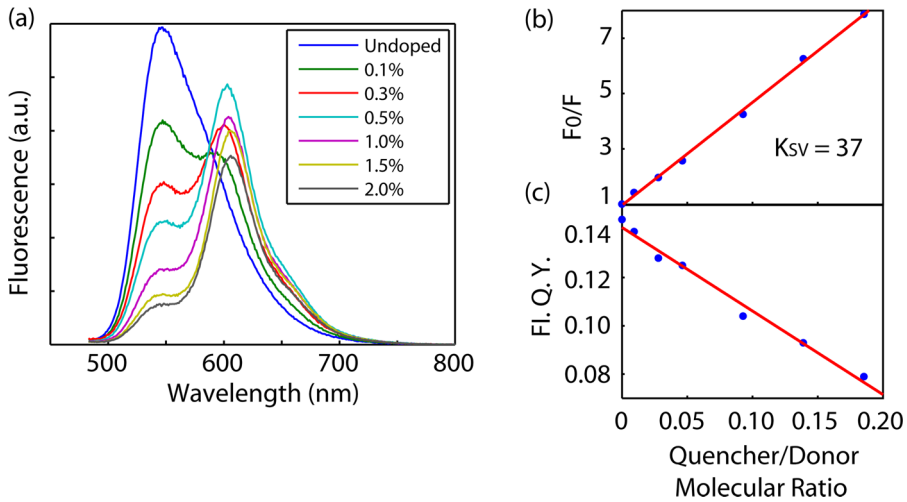

Figure 8. (a) Fluorescence spectra of undoped PFBT CPNs and perylene red doped PFBT CPNs at various dopant percentages. (b) Stern−Volmer quenching plot. (c) Total fluorescence quantum yield at various quencher−donor molecular ratios. Adapted with permission from ref 36. Copyright 2013 American Chemical Society.

quenched by a single perylene red molecule. Assuming that the quenched volume approximately corresponds to a sphere of (37) close-packed molecules, this corresponds to an effective quenching radius of roughly 5.3 nm. This is significantly larger than the Förster radius, which provides some preliminary indication that exciton diffusion or multiple energy transfer likely occurs in this system.

4.2. Time Resolved Fluorescence of PFBT CPNs Doped with Perylene Red

Time-resolved fluorescence provides additional information about energy transfer to the dye. Time-correlated single photon counting (TCSPC) was used to monitor the decay dynamics of the conjugated polymer excited states (i.e., exciton states). Figure 9 shows the fluorescence decay kinetics traces for the PFBT

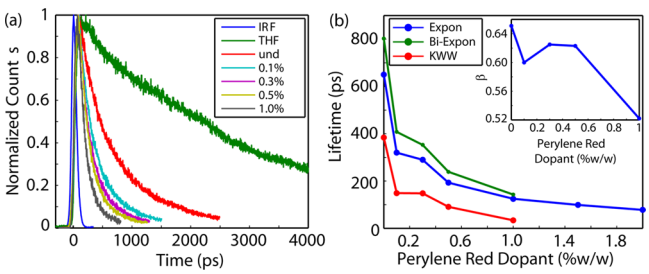

Figure 9. (a) Normalized fluorescence lifetime decay traces for PFBT in THF, undoped PFBT CPNs, and perylene red doped PFBT CPNs. (b) Single exponential (blue), biexponential weighted average (green), and KWW (red) lifetimes of perylene red doped CPNs. The inset shows the stretch parameter β obtained from the KWW lifetime fitting. Adapted with permission from ref 36. Copyright 2013 American Chemical Society.

polymer in THF, for PFBT CPNs suspended in water, and for perylene red-doped PFBT CPNs at various doping levels. While the polymer in THF exhibits roughly single exponential decay, consistent with a homogeneous decay process, the undoped CPNs and the dye-doped CPNs exhibit decays that fit poorly to a single exponential decay, indicating a heterogeneous system with a range of decay rates. The KWW decay function,

$$F(t) = F_0 e^{-(t/\tau)^{\beta}} \tag{25}$$

where τ is a lifetime parameter and β represents qualitatively the width of the lifetime distribution ($\beta = 1$ corresponds to a single lifetime), is widely used for characterizing a variety of systems with heterogeneous dynamics.[131] A biexponential decay function describes a heterogeneous population with two decay constants (i.e., a bimodal distribution), but it can also be used to approximate a more or less continuous distribution of lifetimes over a finite range. Nonlinear least-squares fitting of the TCSPC kinetics traces both to the KWW function and to a biexponential function yielded good quality fits for most CPN samples.

The fluorescence lifetime of the polymer in solution is roughly 3 ns, and the decay fits well to a single exponential, whereas for undoped CPNs the decay is complex, with a weighted average lifetime of 800 ps and a KWW parameter β of 0.65. For the dye-doped CPNs, excited state lifetimes decrease monotonically with increasing doping, as expected for dynamic quenching by the dopant dye. The weighted average lifetime drops from 800 ps for undoped particles to 410 ps at 0.1% doping and 190 ps at 1% doping. The β parameter from the KWW fit varies over the range of about 0.62 to 0.52 over the doping range 0.1 to 1%.

4.3. Fluorescence Quenching in Undoped CPNs

Considering the trends that are evident in the lifetime results, it appears that a quenching process or similar process occurs in undoped CPNs, resulting in a range of exciton decay rates, and that this quenching process likely competes with energy transfer to the dye in the case of the dye-doped CPNs. Several questions emerge about the nature of this quenching process. What is the underlying cause (or causes) of the heterogeneous quenching? Does exciton diffusion increase or decrease heterogeneity? What process or processes cause the roughly factor of 3 lifetime reduction of CPNs dispersed in water as compared to the polymer in an organic solvent? Are there H- or J-aggregate species, and if so, how are they affecting the exciton radiative rate? What are the roles of other quenching species or processes, such as chemical defects or polarons? What is the role of exciton diffusion? How does the presence of defects or other quenching species affect energy transfer to the dopant dyes? How does the presence of quencher species affect the measured exciton diffusion length, and how can we correct for quenching by defects when determining the exciton diffusion length? While it appears that there are too many questions to be answered with

DOI: 10.1021/acs.chemrev.6b00419
Chem. Rev. XXXX, XXX, XXX−XXX

just a few experimental measurements, with the help of a few reasonable assumptions and comparison of experimental results to model calculations, we can obtain provisional answers and a more or less self-consistent physical picture.

Let us first consider the species and processes causing the reduced lifetime of CPNs relative to the polymer in solution, starting with H- and J-aggregates. The fact that both the fluorescence lifetime and the fluorescence quantum yield are reduced in the particles, by roughly the same factor (relative to the polymer in solution), is not consistent with J-aggregate formation, based on the following reasoning. For J-aggregates, the radiative rate typically increases relative to the unaggregated state, resulting in a shorter excited state lifetime and typically an increased or similar quantum yield. However, for the CPNs, the radiative rate obtained by combining the fluorescence quantum yield and lifetime results,

$$k_{rad} = \frac{\varnothing}{\tau} \tag{26}$$

yields similar values for the radiative rate of the CPN as for the polymer dissolved in organic solvent (k_{rad} = 1.2 × 10^8 s^{-1}). Additionally, the UV−vis and fluorescence spectra do not show signs of significantly increased J- or H-aggregate coupling in the nanoparticle state as compared to the polymer dissolved in organic solvent (e.g., large shifts in the spectra or large changes in line shape). While there are most likely some changes in the amount of excitonic coupling upon nanoparticle formation, owing to the higher chromophore density, the results indicate that H- and J-type aggregates are not likely to be the primary cause of the large decrease in lifetime and fluorescence quantum yield upon particle formation. It is possible that other ground-state aggregate species (e.g., dimers, charge transfer species) or excited state aggregate species (e.g., excimers and exciplexes) could be involved. There is no direct spectroscopic evidence of large fractions of such species in the present system; however, even a small fraction of such species could result in significant quenching.

Having ruled out H- and J-aggregate formation as a likely explanation for the lifetime and quantum yield results, we now consider the effects of various quenching species. In addition to the aforementioned nonfluorescent aggregate species, chemical defects and polarons can act as fluorescence quenchers. Several prior results point to hole polarons as the principal quenching species in undoped CPNs. Field-modulation near-field scanning optical microscopy indicated that mobile, positively charge species, likely to be hole polarons, act as fluorescence quenchers in poly[2-methoxy-5-(2-ethylhexyloxy)-1,4-phenylenevinylene] (MEH-PPV) films.[129,130] Fluorescence quantum yield decreases in the presence of oxygen, which is known to act as an electron acceptor that increases polaron concentration.[92] Other examples are discussed above (Section 3.3). Based on these results, we hypothesize that the principal contributor to the increased nonradiative rate in the PFBT CPNs is quenching by hole polarons, which is amplified by multiple energy transfer (exciton diffusion).

4.4. Modeling of Quenching by Polarons

Based on the above analysis indicating quenching by polarons even in undoped CPNs, quenching by polarons was included explicitly in exciton diffusion energy transfer model calculations. Since quenching by dyes is also represented in the calculations, this approach is analogous to the "standard addition" approach used in chemical analysis. An overview of the calculation method is provided above (Section 3.2), and details of the calculation are provided elsewhere.[36] The polaron density and the exciton diffusion length were taken as adjustable fit parameters. Since the Förster radius for the hole polarons is not known, the Förster radius of the perylene red dye (calculated from spectral overlap) was used; thus, the polaron density parameter obtained from the fit does not estimate the actual polaron density, but rather the density of dye molecules needed to obtain similar quenching behavior. Based on simple geometric calculations indicating relatively low quenching by polarons for the polymer in an extended conformation, and the observed single exponential decay of the polymer in organic solvent, it is reasonable to assume that the fluorescence lifetime of the polymer in organic solvent is close to the lifetime of the hypothetical polymer in CPNs in the absence of polaron quenchers. Thus, in the model calculations, the fluorescence lifetime of the polymer in organic solvent was used to represent the lifetime of the polymer in the CPNs, since using the measured lifetime of the undoped CPNs in the calculations, and then adding defect-quenchers to the calculations would constitute double counting.

The fit of the exciton diffusion model calculations and comparison to the experimental results are shown in Figure 10.

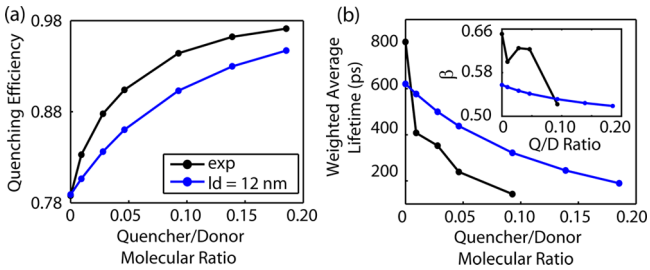

Figure 10. Simulated (blue) and experimental (black) (a) quenching efficiency and (b) average lifetime. (inset) KWW stretch parameter β at various perylene red doping percentages. Adapted with permission from ref 36. Copyright 2013 American Chemical Society.

The best fit parameters were L_D = 12 nm and a defect concentration of 2.3 dye-equivalents per 8 nm diameter nanoparticle, or roughly 6 × 10^{18} cm^{-1}. The L_D obtained is similar to that obtained for conjugated polymer thin films obtained using a different approach. However, when quenching by defects or polarons is removed from the model, the result is closer to 6 nm. This dramatic difference indicates the importance of considering quenching by defects or polarons when using quenching-based approaches to obtain the exciton diffusion length. Indeed, in the limit of a large exciton diffusion length, unless quenching by defects is taken into account, measurements of the effect of quencher dyes on donor fluorescence will give an apparent exciton diffusion length that is roughly the average nearest-neighbor distance between defects. In other words, in some cases the quenching experiments essentially measure defect density, not the exciton diffusion length.

Let us consider whether roughly 2−3 polarons per 8 nm diameter nanoparticle is physically reasonable. If we assume that the chromophore volume is roughly 1 nm^3, there are roughly 200−300 chromophores per nanoparticle, and if we accept another analysis (e.g., dye doping results and single molecule blinking results) indicating roughly 1−30 polarons per nanoparticle, then roughly 1−5% of chromophores are oxidized. Given that the exciton binding energy is typically in the range 200−400 meV for conjugated polymers, some polarons are likely

DOI: 10.1021/acs.chemrev.6b00419
Chem. Rev. XXXX, XXX, XXX−XXX

generated by exciton dissociation. While some fraction of polarons recombine, some can become trapped due to inhomogeneities or trap sites in the polymer. Indeed, substantial trapping of charge carriers has been observed in ultrafast pump-push spectroscopy results.[132,133] For particles suspended in water, water at the particle surface or trapped in the interior of the particle could help stabilize or trap polarons. Additionally, the polymer is likely partially oxidized during the particle preparation process.[134] That said, more than a few percent oxidation would likely have observable effects on the UV−vis absorption spectrum, which puts a limit on the likely degree of oxidation. Considering these facts, as well as the model results, it seems plausible that a few polarons per nanoparticle are present under the experimental conditions and that quenching by the polarons, amplified by exciton diffusion or multiple energy transfer, could explain the exciton lifetime distribution and quantum yield results of undoped CPNs. This conclusion is supported by other experimental results indicating improved fluorescence quantum yield and longer exciton lifetimes when mildly reducing species are added to the CPNs.[92]

Let us examine in more detail how various experimental observables are determined by the various fit parameters. Employing a larger diffusion length L_D increases the amount of quenching (improving the fit to the steady-state fluorescence quenching results and the average lifetime) but leads to a larger β value than that observed experimentally. In the limit of high L_D ($L_D \gg R_0$, where R_0 is the Förster radius), the model yields homogeneous, roughly single exponential decay dynamics ($\beta = 1$), similar to basic diffusion-limited reaction theory. Similarly, reducing L_D resulted in more heterogeneous decay dynamics, which is not surprising, since the Förster energy transfer rate is highly dependent on distance, and there are a range of donor−acceptor distances, resulting in a range of polymer (donor) excited state lifetimes. While both the Förster radius and the exciton diffusion length each contribute to the quenching efficiency or quenching volume per quencher, they both affect the donor polymer lifetime distribution width in opposite ways. Thus, we conclude that steady-state and time-resolved fluorescence results obtained for a series of dopant concentrations, fitted to the exciton diffusion and energy transfer model, can determine the relative contributions of defect (in this case, likely polaron) quenching, exciton diffusion, and Förster transfer. However, while there is qualitative agreement between the model and experimental results, there is clearly much room for improvement. It is likely that there are sources of heterogeneity in the dynamics that are not accounted for in the exciton diffusion and energy transfer model, and including the effects of such heterogeneity in the model could improve the match between the model and experiment. Perhaps single particle spectroscopy studies can help provide additional information about the nature of the heterogeneous dynamics. Additional studies with different conjugated polymers and different acceptor dyes could provide additional tests of the model and also yield important information about additional causes of heterogeneous dynamics. Furthermore, comparison of experimental results to more detailed (i.e., atomistic, quantum-mechanical) models could yield additional information about heterogeneous transport or energy transfer processes.

Finally, let us briefly consider another hypothesis that does not invoke polarons as the principal cause of the reduced quantum yield for CPNs as compared to the polymer dissolved in organic solvent. Higher-level exciton theory indicates that, at higher chromophore densities, there are likely additional exciton decay pathways, such as exciplex formation, exciton fission, etc., due to higher overlap of electronic wave functions as well as quadrupolar coupling.[57] This has been proposed as a possible explanation for the often low fluorescence quantum yield of excitons in organic semiconductors, and as an explanation of the apparent paradox that while the rate of Förster homotransfer (between identical chromophores) should increase with increasing chromophore density, and should result in exciton diffusion lengths on the order of microns for readily achievable chromophore densities of 1 nm^{-3}, the actual measured exciton diffusion lengths are much lower, and typically less than 20 nm for conjugated polymers. While there is most likely an increase in nonradiative decay pathways and associated rates at sufficiently high chromophore densities, such phenomena would most likely yield a uniform increase in nonradiative decay rates and thus does not account for the wide range of decay rates we have observed, which support the notion of a small fraction (a few percent or less) of isolated quenching sites, with typical distances between neighboring sites of several nanometers. Such sites could be polarons, chemical defects, or weakly fluorescent aggregate species, though, as stated above, the evidence seems to point toward polarons in the case of PFBT, MEH-PPV, and similar conjugated polymers. While polarons or other quenching defects are likely to be present for the polymer in solution, the reduced overall rate of energy transfer (between like chromophores, and between chromophores and defects) in solution effectively suppresses quenching (assuming a few percent or fewer quenching sites) in the solution phase, but the onset of significant exciton diffusion in the particle phase (and thin films) results in significant quenching that limits exciton diffusion. That said, the question of what are the key factors limiting exciton diffusion in conjugated polymers is still open, and additional research is needed to settle the matter.

5. POLARON DYNAMICS IN CPNS

As discussed in the previous sections, hole polarons are known to be efficient fluorescence quenchers in conjugated polymer systems. Hole polarons are essentially nonfluorescent with red-shifted absorption spectrum compared to neutral polymers, which results in efficient fluorescence quenching through Förster energy transfer.[40,87] Polaron dynamics are commonly observed in single molecular studies of CPNs and can have great impact on CPNs fluorescence. For example, generation and annihilation of polarons in CPNs result in the fluorescence blinking behavior observed in single CPNs.[14] Also, polaron population in CPNs is likely to vary with excitation power. Abrupt changes in excitation intensity can cause polaron population to increase or decrease, which results in the fluorescence decay and recovery behavior.[26] In addition, the large polaron population presented in CPNs at high excitation intensities likely causes fluorescence saturation behavior.[14,95] It has recently been reported that a hole polaron can effectively quench the local fluorescence and induce a dark spot in a single nanoparticle, which moves with the polaron and results in the displacement of the fluorescence centroid.[37] The fluctuations in the fluorescence centroid thus can be used to track the motion of individual polarons and provide a unique window into charge transport processes in conjugated polymer films and devices. In this section, we will discuss and model various phenomena related to polaron dynamics in CPNs, and experimental results including single particle fluorescence studies, photomodulation studies, as well as single polaron tracking experiments will be summarized.

DOI: 10.1021/acs.chemrev.6b00419
Chem. Rev. XXXX, XXX, XXX−XXX

5.1. Fluorescence Saturation Behavior of CPNs

The effective emission rates of fluorescent molecules at high excitation intensity are often limited by saturation due to the presence of a triplet state or other long-lived, metastable, nonfluorescent, or quencher species. The typical saturated singlet emission rates of single dye molecules are in the range 10^3 to 10^6 s^{-1}, limited by triplet saturation to a value well below the peak emission rate k_r.[135] For CPNs, the saturated emission rates are on the order of 10^8 s^{-1},[14,95] which are at least 2 orders of magnitude higher than those of typical dyes. It is likely that both triplet state quenching and quenching by hole polarons contributed to the fluorescence saturation of CPNs. A previous study indicates that, under the presence of atmospheric O_2, MEH-PPV nanoparticles exhibit saturated emission rates that are ~10 times lower than those obtained under N_2 atmosphere.[26] Since O_2 is known to induce polaron formation in conjugated polymers by accepting an electron from the polymer excited state,[87] it is likely that, in the presence of O_2, the fluorescence saturation of CPNs is mainly due to polarons. To model the fluorescence saturation behavior observed, a set of rate equations were used to describe exciton and polaron population in CPNs. Modifying the conventional fluorescence rate equation to include polaron photogeneration and quenching by polarons yields

$$\frac{dn_{ex}}{dt} = k_{abs} - k_f n_{ex} - k_q n_{ex} n_p - k_{diss} n_{ex} + k_{rec} n_p \tag{27}$$

$$\frac{dn_p}{dt} = k_{diss} n_{ex} - k_{rec} n_p \tag{28}$$

which describe the coupled kinetics of excitons and polarons, where n_{ex} and n_p are the population of excitons and polarons per particle, k_{abs} is the photon absorption rate constant, k_f is the rate constant of radiative and nonradiative relaxation, k_q is the (assumed second-order) rate constant of exciton quenching by polarons, k_{diss} is the rate constant of exciton dissociation to form polarons, and k_{rec} is the recombination rate constant for polarons. The solutions to the above equations are complex expressions, making them difficult to use in data modeling or fitting. There are multiple simplifications that can be applied. Due to efficient energy funneling from excitons to hole polarons,[40,41,87] polarons mainly affect exciton population through the quenching process; thus, the third term in eq 27 is much larger than the last two terms. Therefore, eq 27 can be rewritten as

$$\frac{dn_{ex}}{dt} = k_{abs} - k_f n_{ex} - k_q n_{ex} n_p \tag{29}$$

Also, it can be assumed that a large portion of polarons are directly generated by photoexcitation so that polaron generation rate is proportional to excitation power. Then the polaron kinetics equation can be rewritten as

$$\frac{dn_p}{dt} = k_{abs}\phi - k_{rec} n_p \tag{30}$$

ϕ is the polaron generation quantum yield. Combining the simplified equations, the steady state exciton and polaron population as a function of k_{abs} were obtained.

$$n_p = \frac{k_{abs}\text{Ø}}{k_{rec}} \tag{31}$$

$$n_{ex} = \frac{k_{abs}}{k_f + k_q n_p} = \frac{k_{abs}}{k_f + k_q \frac{k_{abs}\text{Ø}}{k_{rec}}} \tag{32}$$

In eq 32, the numerator corresponds to photon absorption and the denominator shows the competition between fluorescence relaxation and energy transfer to hole polarons. In Figure 11, the

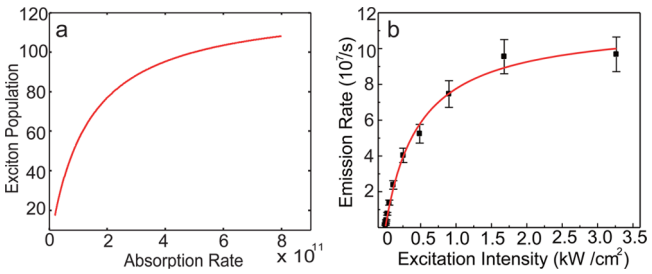

Figure 11. (a) Saturation curve plotted from the steady state solution of eqs 29 and 30. (b) Fluorescence saturation curve of single PFBT particles (black dots) fitted to the equation $F = \frac{I_e/I_s}{1+I_e/I_s}F_\infty$ (red solid line). Adapted with permission from ref 14. Copyright 2008 American Chemical Society.

steady state solution was compared to the experimental data. A PFBT single particle fluorescence saturation curve was fitted to the equation $F = \frac{I_e/I_s}{1+I_e/I_s}F_\infty$ (Figure 11b), where F is the emission intensity at a given power, I_e and I_s are the excitation power and the saturation power, respectively, and F_∞ is the saturation intensity. A calculated saturation curve based on the rate model is shown in Figure 11 a. While we do not know all the parameters in eq 32, there is a range of physically reasonable values that can yield clear saturation behavior. According to the typical fluorescence lifetime of CPNs, $k_f = 10^9$ s^{-1} was used in the calculation. Since quenching by polarons is a competing rate process to fluorescence relaxation, $k_q n_p$ should not be significantly smaller or larger than k_f; therefore, $k_q = 10^8$ s^{-1} was used. k_{abs} ranging from 10^{11} s^{-1} to 10^{12} s^{-1} and $\frac{\text{Ø}}{k_{rec}} = 10^{-11}$ s were employed for the calculation. The generated saturation curve shows good agreement with the experimental data, which suggests a large polaron population at high excitation power as a possible explanation of the fluorescence saturation behavior of CPNs.

5.2. Reversible Fluorescence Decay Process of CPNs

In the single particle study of CPNs, it is commonly observed that the fluorescence of a CPN will undergo a rapid initial decay process followed by a significantly slower decay. Unlike bleaching caused by photochemical degradation of polymer chains, the initial fluorescence decay is recoverable after blocking the excitation light for a period of time.[26] It is hypothesized that the decay and recovery processes are caused by reversible photogeneration and annihilation of quencher species. The population of the quencher is likely dependent on excitation power. When the excitation intensity changes, the quencher population will respond to change and establish a new equilibrium, which results in the fluorescence decay and recovery behavior. These phenomena were further explored by photomodulation experiments, in which the excitation switches between two levels of intensity. The modulation experiments were performed with both bulk CPNs aqueous dispersion and single particles. When the sample was exposed to the air, clear decay processes were

DOI: 10.1021/acs.chemrev.6b00419
Chem. Rev. XXXX, XXX, XXX−XXX

observed at the high excitation intensity and recovery processes were observed at the low excitation intensity (Figure 12a), while,

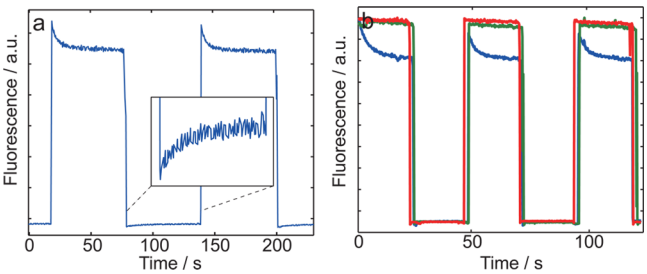

Figure 12. (a) Fluorescence decay and recovery trajectories obtained from excitation intensity modulation of MEH-PPV CPNs aqueous dispersion. (b) Comparison of fluorescence decay and recovery trajectories obtained from MEH-PPV CPNs aqueous dispersion in air (blue), after bubbling with N_2 (green), with addition of 0.01 M DABCO (red). Adapted with permission from ref 26. Copyright 2010 The Royal Society of Chemistry.

under N_2 atmosphere, the excitation modulation induced transitions are nearly completely suppressed (Figure 12b). Similar behavior was observed when a radical scavenging agent, 1,4-diazabicyclo[2,2,2]octane (DABCO), was added to the CPNs dispersion. Since O_2 is known to induce polaron formation in conjugated polymers,[87] the hole polaron is likely to be the quencher species that caused the fluorescence decay and recovery dynamics. In the preliminary analysis, the decay and recovery traces were fitted to single exponential functions. It was observed that the recovery process can be roughly fitted to a single exponential function while the decay process typically does not fit well. There are also noticeable differences between the decay and the recovery time constants obtained from the single exponential fitting. These observations indicate that the decay and recovery processes probably follow different function forms. To further understand these processes, the same set of rate equations that was discussed in the previous section were used to model the population change of exciton and polaron during the photomodulation experiment.

As discussed above, the initial fluorescence intensity decay observed when CPNs were first exposed to the excitation light is likely caused by the growth of the polaron population from 0 to a steady state value. Solving eq 30 gives the analytical solution of the polaron population growth process:

$$n_p(t) = \frac{k_{abs}\emptyset(1 - e^{-k_{rec}t})}{k_{rec}} \tag{33}$$

Since polaron generation/recombination dynamics are much slower than photon absorption and fluorescence relaxation, the exciton population will first reach a steady state before generation of any polaron. The steady state exciton population without quenching by polaron only depends on k_{abs} and k_f:

$$n_{ex} = \frac{k_{abs}}{k_f} \tag{34}$$

Then as the polaron population increases, the exciton population will decay as a function of the polaron population:

$$n_{ex} = \frac{k_{abs}}{k_f + k_q n_p} \tag{35}$$

Combining this relationship with eqs 33 and 35, we obtain the functional form of the initial fluorescence intensity decay.

$$n_{ex}(t) = \frac{1}{\frac{k_f}{k_{abs}} + \frac{k_q\emptyset}{k_{rec}}(1 - e^{-k_{rec}t})} \tag{36}$$

Similarly, both the decay and recovery processes in a photomodulation experiment can be described by solving eqs 29 and 30. The only difference is whether the initial polaron population is smaller or larger than the final steady state value. Let us assume an initial polaron population of n_{p_0} before an excitation intensity transition and solve the equations again:

$$n_{ex}(t) = \frac{1}{\frac{k_f}{k_{abs}} + \frac{k_q\emptyset}{k_{rec}}(1 + ae^{-k_{rec}t})} \tag{37}$$

$$a = \frac{n_{p_0}k_{rec}}{k_{abs}\emptyset} - 1 = \frac{I_{initial}}{I_{final}} - 1 \tag{38}$$

The solution is similar to eq 36 with an additional parameter a that is related to the initial polaron population n_{p_0}, which can be expressed by the ratio of the initial and final excitation powers. When the final excitation power is lower than the initial excitation power, $a > 0$ and we have fluorescence recovery. When the final excitation power is higher than the initial excitation power, $a < 0$ and we have fluorescence decay. When $I_{initial} = 0$, then we have eq 36, which is the special case of polaron population growing from 0 to a steady state value. According to eqs 37 and 38, single particle fluorescence decay and the recovery trajectories were fitted to the functions $y = \frac{1}{a - be^{-cx}}$ and $y = \frac{1}{a + be^{-cx}}$, respectively (Figure 13). The decay function

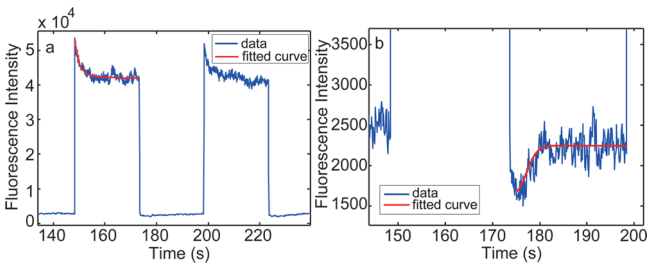

Figure 13. (a) Fluorescence decay and recovery trajectories of a PFBT nanoparticle (blue) with the decay part fitted to the function $y = \frac{1}{a - be^{-cx}}$ (red). (b) Fluorescence recovery trajectory of the same PFBT nanoparticle (blue) with fitting to the function $y = \frac{1}{a + be^{-cx}}$ (red).

$y = \frac{1}{a - be^{-cx}}$ is a discontinuous function with a steep initial decrease, which explains why the decay dynamics deviate from a single exponential fit. The experimental data shows good agreement with the fitted functional forms. From the exponential terms in the fitting, the polaron recombination time constant can be extracted. The fluorescence decay fitting yielded $k_{rec} = 0.1\ s^{-1}$ (Figure 13 a) while the recovery fitting yielded $k_{rec} = 0.08\ s^{-1}$ (Figure 13 b). These results are consistent with the autocorrelation time constants obtained from the analysis of the fluorescence intensity fluctuations of CPNs,[37] which will be discussed in the following section.

DOI: 10.1021/acs.chemrev.6b00419
Chem. Rev. XXXX, XXX, XXX−XXX

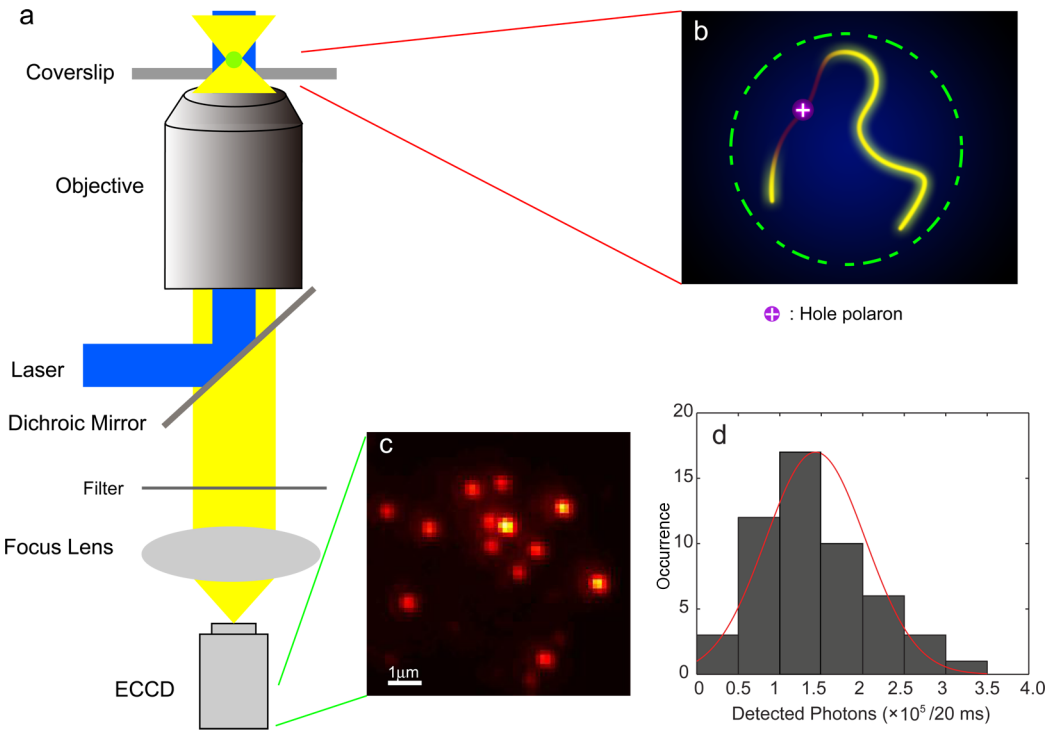

Figure 14. (a) Single polaron tracking microscopy setup. (b) Illustration showing the effect of quenching by a hole polaron on the single CPN fluorescence. (c) Typical fluorescence CCD image of PFBT CPNs. (d) Detected photon histogram for PFBT CPNs at the excitation power of 70 W/cm^2, fitted to a Gaussian distribution (red line). Adapted with permission from ref 37. Copyright 2012 American Chemical Society.

5.3. Tracking Polaron Motion inside CPNs

Single molecule studies of CPNs revealed an interesting phenomenon that CPNs fixed on a coverslip exhibit small movement in the fluorescence spot. There is evidence that a hole polaron quenches the local fluorescence and induces a dark spot in a single nanoparticle.[40,41] As the polaron moves inside the nanoparticle, the fluorescence centroid will also be displaced due to the movement of the dark spot. Based on this phenomenon, a method was proposed to track individual polaron motion inside CPNs with 1 nm spatial resolution,[37] which provides an unprecedented level of detail about charge transport in conjugated polymers.

The polaron tracking experiment was performed on an inverted microscope (Figure 14a). PFBT CPNs with size 15 ± 4 nm were dispersed on a coverslip and excited with a 473 nm laser. The single particle fluorescence was detected using a CCD camera (Figure 14c). Under a moderate excitation power (70 W/cm^2), typically around 10^5 photons were detected per 20 ms exposure (Figure 14d), which yields a 2D localization uncertainty of 0.7 nm.[136] 8000 frames of the fluorescence microscopy images (160 s) were acquired at a frame rate of 50 Hz. To determine the fluorescence centroid, the fluorescence spot of each particle was fitted to a 2D Gaussian function. The fluorescence centroid trajectories obtained show clear fluctuations well above the localization uncertainty. The fluorescence intensity trajectories of the particles also show pronounced fluctuations above the Poisson noise level. The position and intensity trajectories were analyzed with autocorrelation (Figure 15). Both the intensity and position autocorrelation show good fit to biexponential or stretched exponential functions, which indicates that there is a range of time scales. In a 4 s time window, typical time constants from the biexponential fitting to the intensity and position autocorrelation are τ_1 = 0.28 s, τ_2 = 3.8 s, and τ_1 = 0.1 s and τ_2 = 1.8 s, respectively. The fitting parameters also show dependence on the fitting time window; as the time window used for fitting increases, the time constants also tends to increase, indicating dynamics spanning several time scales. Several possible explanations for the dynamics were considered, including quenching by polarons, quenching by triplet excitons, and photochemical degradation of the polymers. According to the autocorrelation time constants, the dynamics observed are

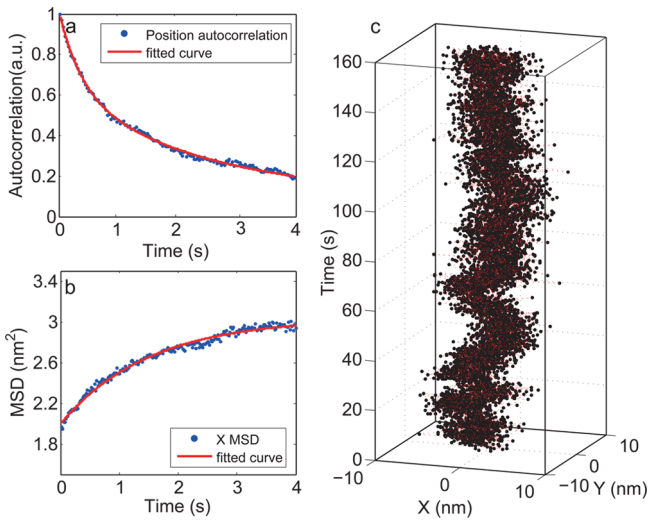

Figure 15. (a) x position autocorrelation curve from 0 to 4 s fitted to the biexponential function ($y = A_1e^{-x/\tau_1} + A_2e^{-x/\tau_2} + y_0$). τ_1 = 0.1 s, τ_2 = 1.60 s, A_1 = 0.2, and A_2 = 0.5. (b) x MSD versus time from 0 to 4.0 s, fitted to the confined diffusion function $\langle x_f^2(\tau)\rangle = \langle x_f^2(0)\rangle + L_f^2\{1 - \exp(-2D_f\tau/L_f^2)\}$ with diffusion coefficient D_f and confinement length L_f of 1.8 nm^2/s and 1.50 nm, respectively. (c) 3D trajectory of the centroid position of a CPN.

DOI: 10.1021/acs.chemrev.6b00419
Chem. Rev. XXXX, XXX, XXX−XXX

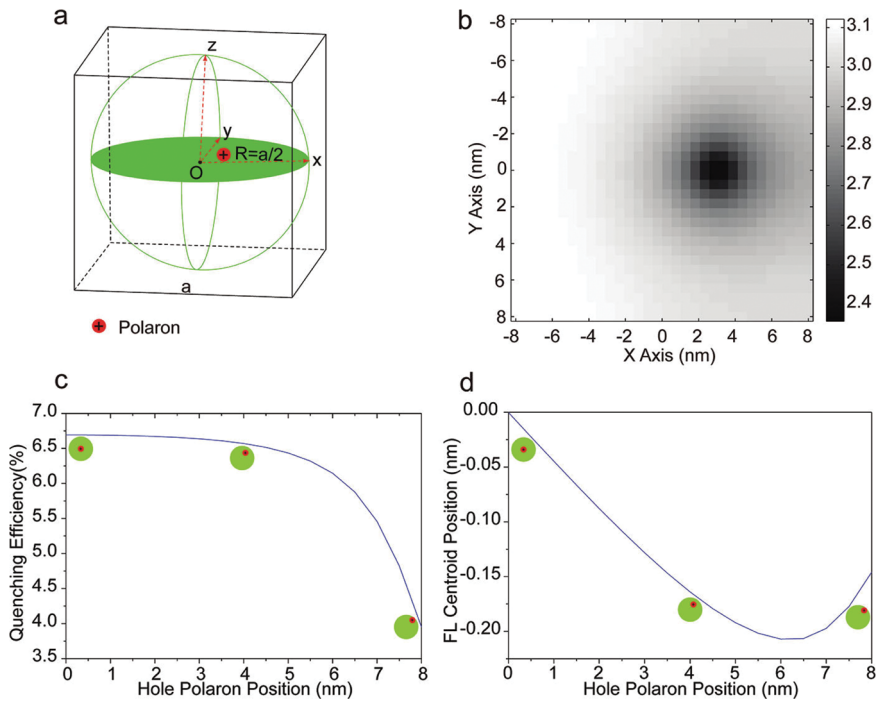

Figure 16. (a) Plot showing a single hole polaron within a 16 nm CPN. (b) Simulated near-field fluorescence showing the exciton density along the *x*, *y* axes with a dark spot caused by energy transfer to a hole polaron. (c) Plot of the simulated quenching efficiency versus polaron position. (d) Simulated fluorescence centroid position versus polaron position. Adapted with permission from ref 37. Copyright 2012 American Chemical Society.

significantly slower than triplet dynamics while they are in range with the time scale of polaron dynamics previously observed in single polymer chains.[125,127] In addition, since most of the fluorescence intensity trajectories show no obvious photobleaching and the majority of the intensity fluctuations are reversible, photochemical degradation is unlikely to be the major cause of the dynamics. The mean square displacement (MSD) exhibits confined diffusion behavior that the MSD starts off linear and then flattens after 1−5 s, which agrees with the physical picture of one or a few charge carriers trapped inside a nanoparticle. Combining all the evidence, we concluded that the fluorescence intensity and centroid position fluctuations observed are likely caused by polaron dynamics. The difference between intensity and position autocorrelation time constants is probably due to the fact that the fluorescence centroid position is mostly affected by polaron motion while the fluorescence intensity is more sensitive to polaron generation and recombination dynamics.

To model the effect of quenching by polaron on the fluorescence centroid of a CPN, exciton diffusion and energy transfer to a hole polaron on a 3D lattice was simulated, similar to the exciton random walk model discussed earlier in the review.[31,36] The polaron was placed at various distances from the center of the grid. For each polaron position, the quenching efficiency and centroid displacement were calculated. The simulated results are shown in Figure 16. It is observed that when the polaron is away from the particle surface, the quenching efficiency of the polaron shows only minor variation at different positions and the centroid displacement follows a linear relationship with the polaron position.

$$\delta x_f = -x_p Q_p \tag{39}$$

where δx_f is the displacement of the fluorescent centroid, x_p is the position of the polaron relative to the center of the particle, and Q_p is the quenching efficiency of a single polaron. However, when the polaron is within 2 nm of the particle surface, the quenching efficiency drops due to lower chromophore density at the surface. As a result, in this region, the relationship between the polaron position and the centroid displacement becomes complex. However, since eq 39 is still valid for 80% of the positions in CPNs, we can use it to roughly estimate charge transport parameters in CPNs.

From fitting the MSD to a confined diffusion function, the diffusion coefficients of the fluorescence centroid D_f were obtained, which range from 10^{-13} to 10^{-14} cm^2/s. Since the diffusion coefficient is related to the square of the displacement, we can convert the diffusion coefficient of the centroid to the diffusion coefficient of the polarons using the relationship $D_p = D_f/Q_p^2$. Since generation and recombination of polarons are known to cause fluorescence blinking behavior, we can estimate Q_p from the fluctuation amplitude of the intensity trajectories. Typical Q_p values obtained from the analysis range from 3 to 15%. Based on these values, we estimated the polaron diffusion coefficients in CPNs to be around 10^{-11}−10^{-12} cm^2/s. Applying the Stokes−Einstein equation, zero field polaron mobilities ranging from 10^{-10} −10^{-9} cm^2 /V s were obtained, which indicates a high level of disorder in CPNs. The polaron mobilities obtained are 1 or 2 orders of magnitude lower than the polaron mobilities reported from voltage−current analysis of the corresponding polymer films.[137,138] Since charge transport in disordered material typically spans over a broad range of time scales,[139,140] the inconsistency is likely to be caused by the limited temporal resolution employed. In addition, the continuous rolling fluctuations observed in the position trajectories also indicate that there might be small step hopping events happening on shorter time scales. To obtain a more detailed picture about the charge transport process in CPNs, polaron tracking with faster framerates is required in future research.

DOI: 10.1021/acs.chemrev.6b00419
Chem. Rev. XXXX, XXX, XXX−XXX

6. CONCLUSIONS

In conclusion, there has been significant recent progress in developing a preliminary understanding of the key processes that determine exciton diffusion and the process of amplified energy transfer or multiple energy transfer to acceptor dyes in conjugated polymer nanoparticles. However, while exciton diffusion in organic crystals and films has been studied for several decades, relatively few such studies have been performed in conjugated polymer nanoparticles, and the field is in its early stages. Interest in exciton diffusion and its effect on the optical properties of heterogeneous, doped, or blended CPNs is largely motivated by a desire to improve the properties of CPNs or "polydots" for various imaging and sensing applications, owing to their exceptional brightness as compared to other particles in the 3−20 nm size range.[26] CPNs are also of interest for possible use in other applications, such as thin film optoelectronic devices. Additionally, CPNs are an interesting model system in that they have properties intermediate between or a composite of free molecules in solution and thin film or bulk, and can thus help provide insight into the interactions that distinguish film properties from those of molecules in solution. CPNs have the extraordinary ability to serve as a "nanoscale window" into exciton transport processes and charge transport processes in conjugated polymer films—by limiting the size to the nanometer scale, we can apply single particle techniques to probe energy transfer to single dyes and the motion of a single charge carrier.[37,95] Ensemble studies of exciton dynamics of CPNs at the picosecond and femtosecond time scales[36,42] have already begun to yield important answers about the nature of exciton diffusion and amplified energy transfer processes. In particular, time-resolved fluorescence spectroscopy of doped CPNs, interpreted using model calculations, has elucidated the important role of quenching by polarons and has yielded approaches to quantifying polaron quenching and its effect on exciton diffusion. This understanding helps to identify possible approaches to suppress polaron quenching effects, such as by addition of mild reducing agents to reduce hole polaron formation (i.e., to control redox balance) or by adding dye acceptors that provide a competitive energy transfer pathway.

While some of the results obtained thus far seem to have already had an impact on our understanding of important phenomena in conjugated polymers and related systems, it is clear that investigations of energy transfer phenomena in conjugated polymer nanoparticles are at an early phase and much remains to be learned. Researchers are currently developing novel single particle-based approaches for exploring energy transfer and exciton diffusion phenomena in CPNs. Additional simulation work is likely to help elucidate how nanoscale structure, heterogeneity, and disorder affect exciton transport, as well as shedding light on such fundamental questions as what is the distribution of exciton sizes in conjugated polymers, what is the distribution of chromophore coupling strengths, what is the distribution of exciton energies, and what is the distribution of energy transfer distances between chromophores or excitons. Further improvements in the control of CPN structure and composition, driven in part by potential applications, could help provide improved results of spectroscopic experiments. Some studies of PT nanoparticles with well-defined structures have already shown interesting results.[84,119,141] However, the physical picture remains unclear, particularly with respect to the role of energy transfer. In particular, the low fluorescence quantum yield of PT nanoparticles complicates analysis—for such highly quenched fluorescence, impurities or chemical defects could be largely responsible for the observed effects. In addition, the high nonradiative relaxation rates relative to exciton homotransfer rates preclude study of exciton diffusion processes. Additional studies, perhaps involving PT and oligothiophene particles in which the interchain interactions or other interactions involved in nonradiative relaxation are significantly reduced, could greatly add to our understanding of nanoscale interactions of chromophores in π-conjugated materials. Hopefully, these efforts will lead to a more accurate nanoscale picture and understanding of the various species, processes, and interactions (and the corresponding time scales) that determine the optical and electronic properties of conjugated polymers. This knowledge could form the basis of additional efforts to develop better CPNs for imaging and sensing, and perhaps eventually help to improve the efficiency of conjugated polymer-based devices.

AUTHOR INFORMATION

Corresponding Author

* Email: mcneill@clemson.edu.

ORCID

Jason McNeill: 0000-0003-2568-8174

Notes

The authors declare no competing financial interest.

Biographies

Yifei Jiang earned his Bachelor's degree in Chemical Physics from University of Science and Technology of China (USTC). As an undergraduate student, he spent one year in Prof. Yanxia Chen's group at Hefei National Laboratory for Physical Sciences, where he learned about electrochemistry and spectroscopy. He received the Undergraduate Research Award from USTC in 2010. He is currently a Ph.D. student in Prof. Jason McNeill's group at Clemson University. His current research focused on photophysical properties of conjugated polymer nanoparticles and their applications in particle tracking and superresolution microscopy.

Jason McNeill earned a Bachelor's degree in Chemistry from Northern Illinois University and a Ph.D. in Physical Chemistry from the University of California, Berkeley, specializing in the area of ultrafast laser spectroscopy of surfaces. He did postdoctoral research with Paul Barbara at the University of Texas, Austin, involving near-field microscopy and single molecule fluorescence spectroscopy. He is currently a member of the faculty in the Department of Chemistry at Clemson University. He is a recipient of the CAREER award from the US National Science Foundation. His research interests include single molecule spectroscopy, the development of novel fluorescent nanoparticles for imaging and sensing applications, and investigating the physics of conjugated polymers.

ACKNOWLEDGMENTS

We acknowledge financial support from the NSF under Grant No. CHE-1412694. We also thank the American Chemical Society, the Royal Society of Chemistry, Macmillan Publisher Ltd, and Wiley-VCH for granting permission to reproduce figures.

REFERENCES

(1) Braun, D.; Heeger, A. J. Visible Light Emission from Semiconducting Polymer Diodes. *Appl. Phys. Lett.* **1991**, *58* (18), 1982−1984.

DOI: 10.1021/acs.chemrev.6b00419
Chem. Rev. XXXX, XXX, XXX−XXX

(2) Sariciftci, N.; Smilowitz, L.; Heeger, A. J.; Wudl, F. Photoinduced Electron Transfer from a Conducting Polymer to Buckminsterfullerene. *Science* **1992**, *258* (5087), 1474−1476.
(3) Sirringhaus, H.; Tessler, N.; Friend, R. H. Integrated Optoelectronic Devices Based on Conjugated Polymers. *Science* **1998**, *280* (5370), 1741−1744.
(4) Friend, R.; Gymer, R.; Holmes, A.; Burroughes, J.; Marks, R.; Taliani, C.; Bradley, D.; Dos Santos, D.; Bredas, J.; Lögdlund, M. Electroluminescence in Conjugated Polymers. *Nature* **1999**, *397* (6715), 121−128.
(5) Salaneck, W. R.; Stafstrom, S.; Brédas, J. L. *Conjugated Polymer Surfaces and Interfaces: Electronic and Chemical Structure of Interfaces for Polymer Light Emitting Devices*; Cambridge University Press: 2003.
(6) Günes, S.; Neugebauer, H.; Sariciftci, N. S. Conjugated Polymer-Based Organic Solar Cells. *Chem. Rev.* **2007**, *107* (4), 1324−1338.
(7) Whitehead, K.; Grell, M.; Bradley, D.; Jandke, M.; Strohriegl, P. Highly Polarized Blue Electroluminescence from Homogeneously Aligned Films of Poly(9, 9-dioctylfluorene). *Appl. Phys. Lett.* **2000**, *76* (20), 2946−2948.
(8) Tessler, N.; Medvedev, V.; Kazes, M.; Kan, S.; Banin, U. Efficient Near-Infrared Polymer Nanocrystal Light-Emitting Diodes. *Science* **2002**, *295* (5559), 1506−1508.
(9) Shirakawa, H.; Louis, E. J.; MacDiarmid, A. G.; Chiang, C. K.; Heeger, A. J. Synthesis of Electrically Conducting Organic Polymers: Halogen Derivatives of Polyacetylene, (CH)x. *J. Chem. Soc., Chem. Commun.* **1977**, *16*, 578−580.
(10) Wudl, F. The Chemical Properties of Buckminsterfullerene (C_{60}) and the Birth and Infancy of Fulleroids. *Acc. Chem. Res.* **1992**, *25* (3), 157−161.
(11) McCullough, R. D.; Lowe, R. D.; Jayaraman, M.; Anderson, D. L. Design, Synthesis, and Control of Conducting Polymer Architectures: Structurally Homogeneous Poly(3-alkylthiophenes). *J. Org. Chem.* **1993**, *58* (4), 904−912.
(12) Bao, Z.; Dodabalapur, A.; Lovinger, A. J. Soluble and Processable Regioregular Poly(3-hexylthiophene) for Thin Film Field-Effect Transistor Applications with High Mobility. *Appl. Phys. Lett.* **1996**, *69* (26), 4108−4110.
(13) Szymanski, C.; Wu, C.; Hooper, J.; Salazar, M. A.; Perdomo, A.; Dukes, A.; McNeill, J. Single Molecule Nanoparticles of the Conjugated Polymer MEH-PPV, Preparation and Characterization by Near-Field Scanning Optical Microscopy. *J. Phys. Chem. B* **2005**, *109* (18), 8543−8546.
(14) Wu, C.; Bull, B.; Szymanski, C.; Christensen, K.; McNeill, J. Multicolor Conjugated Polymer Dots for Biological Fluorescence Imaging. *ACS Nano* **2008**, *2* (11), 2415−2423.
(15) Yu, J.; Wu, C.; Sahu, S. P.; Fernando, L. P.; Szymanski, C.; McNeill, J. Nanoscale 3D Tracking with Conjugated Polymer Nanoparticles. *J. Am. Chem. Soc.* **2009**, *131* (51), 18410−18414.
(16) Wu, C.; Schneider, T.; Zeigler, M.; Yu, J.; Schiro, P. G.; Burnham, D. R.; McNeill, J. D.; Chiu, D. T. Bioconjugation of Ultrabright Semiconducting Polymer Dots for Specific Cellular Targeting. *J. Am. Chem. Soc.* **2010**, *132* (43), 15410−15417.
(17) Wu, C.; Hansen, S. J.; Hou, Q.; Yu, J.; Zeigler, M.; Jin, Y.; Burnham, D. R.; McNeill, J. D.; Olson, J. M.; Chiu, D. T. Design of Highly Emissive Polymer Dot Bioconjugates for in Vivo Tumor Targeting. *Angew. Chem., Int. Ed.* **2011**, *50* (15), 3430−3434.
(18) Duarte, A.; Pu, K.-Y.; Liu, B.; Bazan, G. C. Recent Advances in Conjugated Polyelectrolytes for Emerging Optoelectronic Applications. *Chem. Mater.* **2011**, *23* (3), 501−515.
(19) Whitcombe, M. J.; Chianella, I.; Larcombe, L.; Piletsky, S. A.; Noble, J.; Porter, R.; Horgan, A. The Rational Development of Molecularly Imprinted Polymer-Based Sensors for Protein Detection. *Chem. Soc. Rev.* **2011**, *40* (3), 1547−1571.
(20) McQuade, D. T.; Pullen, A. E.; Swager, T. M. Conjugated Polymer-Based Chemical Sensors. *Chem. Rev.* **2000**, *100* (7), 2537−2574.
(21) Thomas, S. W.; Joly, G. D.; Swager, T. M. Chemical Sensors Based on Amplifying Fluorescent Conjugated Polymers. *Chem. Rev.* **2007**, *107* (4), 1339−1386.
(22) Wu, C.; Bull, B.; Christensen, K.; McNeill, J. Ratiometric Single-Nanoparticle Oxygen Sensors for Biological Imaging. *Angew. Chem., Int. Ed.* **2009**, *48* (15), 2741−2745.
(23) Ye, F.; Wu, C.; Jin, Y.; Chan, Y.-H.; Zhang, X.; Chiu, D. T. Ratiometric Temperature Sensing with Semiconducting Polymer Dots. *J. Am. Chem. Soc.* **2011**, *133* (21), 8146−8149.
(24) Chan, Y.-H.; Wu, C.; Ye, F.; Jin, Y.; Smith, P. B.; Chiu, D. T. Development of Ultrabright Semiconducting Polymer Dots for Ratiometric PH Sensing. *Anal. Chem.* **2011**, *83* (4), 1448−1455.
(25) Ye, F.; Sun, W.; Zhang, Y.; Wu, C.; Zhang, X.; Yu, J.; Rong, Y.; Zhang, M.; Chiu, D. T. Single-Chain Semiconducting Polymer Dots. *Langmuir* **2015**, *31* (1), 499−505.
(26) Tian, Z.; Yu, J.; Wu, C.; Szymanski, C.; McNeill, J. Amplified Energy Transfer in Conjugated Polymer Nanoparticle Tags and Sensors. *Nanoscale* **2010**, *2* (10), 1999−2011.
(27) Harbron, E. J.; Davis, C. M.; Campbell, J. K.; Allred, R. M.; Kovary, M. T.; Economou, N. J. Photochromic Dye-Doped Conjugated Polymer Nanoparticles: Photomodulated Emission and Nanoenvironmental Characterization. *J. Phys. Chem. C* **2009**, *113* (31), 13707−13714.
(28) Chan, Y.-H.; Gallina, M. E.; Zhang, X.; Wu, I.-C.; Jin, Y.; Sun, W.; Chiu, D. T. Reversible Photoswitching of Spiropyran-Conjugated Semiconducting Polymer Dots. *Anal. Chem.* **2012**, *84* (21), 9431−9438.
(29) Betzig, E.; Patterson, G. H.; Sougrat, R.; Lindwasser, O. W.; Olenych, S.; Bonifacino, J. S.; Davidson, M. W.; Lippincott-Schwartz, J.; Hess, H. F. Imaging Intracellular Fluorescent Proteins at Nanometer Resolution. *Science* **2006**, *313* (5793), 1642−1645.
(30) Rust, M. J.; Bates, M.; Zhuang, X. Sub-Diffraction-Limit Imaging by Stochastic Optical Reconstruction Microscopy (STORM). *Nat. Methods* **2006**, *3* (10), 793−796.
(31) Wu, C.; Zheng, Y.; Szymanski, C.; McNeill, J. Energy Transfer in a Nanoscale Multichromophoric System: Fluorescent Dye-Doped Conjugated Polymer Nanoparticles. *J. Phys. Chem. C* **2008**, *112* (6), 1772−1781.
(32) Jin, Y.; Ye, F.; Zeigler, M.; Wu, C.; Chiu, D. T. Near-Infrared Fluorescent Dye-Doped Semiconducting Polymer Dots. *ACS Nano* **2011**, *5* (2), 1468−1475.
(33) Kietzke, T.; Neher, D.; Landfester, K.; Montenegro, R.; Güntner, R.; Scherf, U. Novel Approaches to Polymer Blends Based on Polymer Nanoparticles. *Nat. Mater.* **2003**, *2* (6), 408−412.
(34) Kietzke, T.; Neher, D.; Kumke, M.; Montenegro, R.; Landfester, K.; Scherf, U. A Nanoparticle Approach to Control the Phase Separation in Polyfluorene Photovoltaic Devices. *Macromolecules* **2004**, *37* (13), 4882−4890.
(35) Piok, T.; Plank, H.; Mauthner, G.; Gamerith, S.; Gadermaier, C.; Wenzl, F. P.; Patil, S.; Montenegro, R.; Bouguettaya, M.; Reynolds, J. R. Solution Processed Conjugated Polymer Multilayer Structures for Light Emitting Devices. *Jpn. J. Appl. Phys.* **2005**, *44* (1B), 479.
(36) Groff, L. C.; Wang, X.; McNeill, J. D. Measurement of Exciton Transport in Conjugated Polymer Nanoparticles. *J. Phys. Chem. C* **2013**, *117* (48), 25748−25755.
(37) Yu, J.; Wu, C.; Tian, Z.; McNeill, J. Tracking of Single Charge Carriers in a Conjugated Polymer Nanoparticle. *Nano Lett.* **2012**, *12* (3), 1300−1306.
(38) Bolinger, J. C.; Traub, M. C.; Adachi, T.; Barbara, P. F. Ultralong-Range Polaron-Induced Quenching of Excitons in Isolated Conjugated Polymers. *Science* **2011**, *331* (6017), 565−567.
(39) Hu, Z.; Gesquiere, A. J. Charge Trapping and Storage by Composite P3HT/PC_{60}BM Nanoparticles Investigated by Fluorescence-Voltage/Single Particle Spectroscopy. *J. Am. Chem. Soc.* **2011**, *133* (51), 20850−20856.
(40) Yu, J.; Song, N. W.; McNeill, J. D.; Barbara, P. F. Efficient Exciton Quenching by Hole Polarons in the Conjugated Polymer MEH-PPV. *Isr. J. Chem.* **2004**, *44* (1−3), 127−132.
(41) Gesquiere, A. J.; Park, S.-J.; Barbara, P. F. Hole-Induced Quenching of Triplet and Singlet Excitons in Conjugated Polymers. *J. Am. Chem. Soc.* **2005**, *127* (26), 9556−9560.

DOI: 10.1021/acs.chemrev.6b00419
Chem. Rev. XXXX, XXX, XXX−XXX

(42) Collini, E.; Scholes, G. D. Coherent Intrachain Energy Migration in a Conjugated Polymer at Room Temperature. *Science* **2009**, *323* (5912), 369−373.
(43) Wang, X.; Groff, L. C.; McNeill, J. D. Multiple Energy Transfer Dynamics in Blended Conjugated Polymer Nanoparticles. *J. Phys. Chem. C* **2014**, *118* (44), 25731−25739.
(44) Wu, C.; McNeill, J. Swelling-Controlled Polymer Phase and Fluorescence Properties of Polyfluorene Nanoparticles. *Langmuir* **2008**, *24* (11), 5855−5861.
(45) Hu, Z.; Tenery, D.; Bonner, M. S.; Gesquiere, A. J. Correlation between Spectroscopic and Morphological Properties of Composite P3HT/PCBM Nanoparticles Studied by Single Particle Spectroscopy. *J. Lumin.* **2010**, *130* (5), 771−780.
(46) Labastide, J. A.; Baghgar, M.; Dujovne, I.; Venkatraman, B. H.; Ramsdell, D. C.; Venkataraman, D.; Barnes, M. D. Time-and Polarization-Resolved Photoluminescence of Individual Semicrystalline Polythiophene (P3HT) Nanoparticles. *J. Phys. Chem. Lett.* **2011**, *2* (17), 2089−2093.
(47) Yang, Z.; Huck, W. T.; Clarke, S. M.; Tajbakhsh, A. R.; Terentjev, E. M. Shape-Memory Nanoparticles from Inherently Non-Spherical Polymer Colloids. *Nat. Mater.* **2005**, *4* (6), 486−490.
(48) Maskey, S.; Osti, N. C.; Perahia, D.; Grest, G. S. Internal Correlations and Stability of Polydots, Soft Conjugated Polymeric Nanoparticles. *ACS Macro Lett.* **2013**, *2* (8), 700−704.
(49) Yan, M.; Rothberg, L.; Papadimitrakopoulos, F.; Galvin, M.; Miller, T. Defect Quenching of Conjugated Polymer Luminescence. *Phys. Rev. Lett.* **1994**, *73* (5), 744.
(50) Huser, T.; Yan, M.; Rothberg, L. J. Single Chain Spectroscopy of Conformational Dependence of Conjugated Polymer Photophysics. *Proc. Natl. Acad. Sci. U. S. A.* **2000**, *97* (21), 11187−11191.
(51) Hu, D.; Yu, J.; Wong, K.; Bagchi, B.; Rossky, P. J.; Barbara, P. F. Collapse of Stiff Conjugated Polymers with Chemical Defects into Ordered, Cylindrical Conformations. *Nature* **2000**, *405* (6790), 1030−1033.
(52) Bolinger, J. C.; Traub, M. C.; Brazard, J.; Adachi, T.; Barbara, P. F.; Vanden Bout, D. A. Conformation and Energy Transfer in Single Conjugated Polymers. *Acc. Chem. Res.* **2012**, *45* (11), 1992−2001.
(53) Adachi, T.; Lakhwani, G.; Traub, M. C.; Ono, R. J.; Bielawski, C. W.; Barbara, P. F.; Vanden Bout, D. A. Conformational Effect on Energy Transfer in Single Polythiophene Chains. *J. Phys. Chem. B* **2012**, *116* (32), 9866−9872.
(54) Yan, M.; Rothberg, L.; Papadimitrakopoulos, F.; Galvin, M.; Miller, T. Spatially Indirect Excitons as Primary Photoexcitations in Conjugated Polymers. *Phys. Rev. Lett.* **1994**, *72* (7), 1104.
(55) Yan, M.; Rothberg, L.; Kwock, E.; Miller, T. Interchain Excitations in Conjugated Polymers. *Phys. Rev. Lett.* **1995**, *75* (10), 1992.
(56) Scholes, G. D.; Rumbles, G. Excitons in Nanoscale Systems. *Nat. Mater.* **2006**, *5* (9), 683−696.
(57) Bardeen, C. J. The Structure and Dynamics of Molecular Excitons. *Annu. Rev. Phys. Chem.* **2014**, *65*, 127−148.
(58) Spano, F. C. Excitons in Conjugated Oligomer Aggregates, Films, and Crystals. *Annu. Rev. Phys. Chem.* **2006**, *57*, 217−243.
(59) Lunt, R. R.; Giebink, N. C.; Belak, A. A.; Benziger, J. B.; Forrest, S. R. Exciton Diffusion Lengths of Organic Semiconductor Thin Films Measured by Spectrally Resolved Photoluminescence Quenching. *J. Appl. Phys.* **2009**, *105* (5), 053711.
(60) Emelianova, E.; Athanasopoulos, S.; Silbey, R. J.; Beljonne, D. 2D Excitons as Primary Energy Carriers in Organic Crystals: The Case of Oligoacenes. *Phys. Rev. Lett.* **2010**, *104* (20), 206405.
(61) Perahia, D.; Traiphol, R.; Bunz, U. H. From Single Molecules to Aggregates to Gels in Dilute Solution: Self-Organization of Nanoscale Rodlike Molecules. *J. Chem. Phys.* **2002**, *117* (4), 1827−1832.
(62) Maskey, S.; Pierce, F.; Perahia, D.; Grest, G. S. Conformational Study of a Single Molecule of Poly Para Phenylene Ethynylenes in Dilute Solutions. *J. Chem. Phys.* **2011**, *134* (24), 244906.
(63) Lim, K.; Fincher, C., Jr; Heeger, A. Rod-to-Coil Transition of a Conjugated Polymer in Solution. *Phys. Rev. Lett.* **1983**, *50* (24), 1934.
(64) Cotts, P. M.; Swager, T. M.; Zhou, Q. Equilibrium Flexibility of a Rigid Linear Conjugated Polymer. *Macromolecules* **1996**, *29* (23), 7323−7328.
(65) Zhou, Y.; Karplus, M.; Wichert, J. M.; Hall, C. K. Equilibrium Thermodynamics of Homopolymers and Clusters: Molecular Dynamics and Monte Carlo Simulations of Systems with Square-Well Interactions. *J. Chem. Phys.* **1997**, *107* (24), 10691−10708.
(66) Noguchi, H.; Yoshikawa, K. Morphological Variation in a Collapsed Single Homopolymer Chain. *J. Chem. Phys.* **1998**, *109* (12), 5070−5077.
(67) Ivanov, V.; Paul, W.; Binder, K. Finite Chain Length Effects on the Coil-Globule Transition of Stiff-Chain Macromolecules: A Monte Carlo Simulation. *J. Chem. Phys.* **1998**, *109* (13), 5659−5669.
(68) Zhang, W.; Smith, J.; Watkins, S. E.; Gysel, R.; McGehee, M.; Salleo, A.; Kirkpatrick, J.; Ashraf, S.; Anthopoulos, T.; Heeney, M. Indacenodithiophene Semiconducting Polymers for High-Performance, Air-Stable Transistors. *J. Am. Chem. Soc.* **2010**, *132* (33), 11437−11439.
(69) Liu, J.; Zhang, R.; Sauvé, G.; Kowalewski, T.; McCullough, R. D. Highly Disordered Polymer Field Effect Transistors: N-Alkyl Dithieno-[3,2-b:2′,3′-d]pyrrole-Based Copolymers with Surprisingly High Charge Carrier Mobilities. *J. Am. Chem. Soc.* **2008**, *130* (39), 13167−13176.
(70) Hugger, S.; Thomann, R.; Heinzel, T.; Thurn-Albrecht, T. Semicrystalline Morphology in Thin Films of Poly(3-hexylthiophene). *Colloid Polym. Sci.* **2004**, *282* (8), 932−938.
(71) Brinkmann, M.; Wittmann, J. C. Orientation of Regioregular Poly(3-hexylthiophene) by Directional Solidification: A Simple Method to Reveal the Semicrystalline Structure of a Conjugated Polymer. *Adv. Mater.* **2006**, *18* (7), 860−863.
(72) Scharsich, C.; Lohwasser, R. H.; Sommer, M.; Asawapirom, U.; Scherf, U.; Thelakkat, M.; Neher, D.; Köhler, A. Control of Aggregate Formation in Poly(3-hexylthiophene) by Solvent, Molecular Weight, and Synthetic Method. *J. Polym. Sci., Part B: Polym. Phys.* **2012**, *50* (6), 442−453.
(73) Panzer, F.; Bässler, H.; Lohwasser, R.; Thelakkat, M.; Köhler, A. The Impact of Polydispersity and Molecular Weight on the Order-Disorder Transition in Poly(3-hexylthiophene). *J. Phys. Chem. Lett.* **2014**, *5* (15), 2742−2747.
(74) Sirringhaus, H.; Wilson, R.; Friend, R.; Inbasekaran, M.; Wu, W.; Woo, E.; Grell, M.; Bradley, D. Mobility Enhancement in Conjugated Polymer Field-Effect Transistors through Chain Alignment in a Liquid-Crystalline Phase. *Appl. Phys. Lett.* **2000**, *77* (3), 406−408.
(75) McCulloch, I.; Heeney, M.; Bailey, C.; Genevicius, K.; MacDonald, I.; Shkunov, M.; Sparrowe, D.; Tierney, S.; Wagner, R.; Zhang, W. Liquid-Crystalline Semiconducting Polymers with High Charge-Carrier Mobility. *Nat. Mater.* **2006**, *5* (4), 328−333.
(76) Gettinger, C.; Heeger, A.; Drake, J.; Pine, D. A Photoluminescence Study of Poly(phenylene vinylene) Derivatives: The Effect of Intrinsic Persistence Length. *J. Chem. Phys.* **1994**, *101* (2), 1673−1678.
(77) Schwartz, B. J. Conjugated Polymers as Molecular Materials: How Chain Conformation and Film Morphology Influence Energy Transfer and Interchain Interactions. *Annu. Rev. Phys. Chem.* **2003**, *54* (1), 141−172.
(78) Roux, C.; Bergeron, J. Y.; Leclerc, M. Thermochromic Properties of Polythiophenes: Structural Aspects. *Makromol. Chem.* **1993**, *194* (3), 869−877.
(79) Wong, K. F.; Skaf, M. S.; Yang, C.-Y.; Rossky, P. J.; Bagchi, B.; Hu, D.; Yu, J.; Barbara, P. F. Structural and Electronic Characterization of Chemical and Conformational Defects in Conjugated Polymers. *J. Phys. Chem. B* **2001**, *105* (26), 6103−6107.
(80) Fried, J. R. *Polymer Science and Technology*; Pearson Education: 2014.
(81) Nguyen, T.-Q.; Doan, V.; Schwartz, B. J. Conjugated Polymer Aggregates in Solution: Control of Interchain Interactions. *J. Chem. Phys.* **1999**, *110* (8), 4068−4078.
(82) Kim, D.; Han, J. T.; Park, Y.; Jang, Y.; Cho, J.; Hwang, M.; Cho, K. Single-Crystal Polythiophene Microwires Grown by Self-Assembly. *Adv. Mater.* **2006**, *18* (6), 719−723.

DOI: 10.1021/acs.chemrev.6b00419
Chem. Rev. XXXX, XXX, XXX−XXX

(83) Briseno, A. L.; Mannsfeld, S. C.; Shamberger, P. J.; Ohuchi, F. S.; Bao, Z.; Jenekhe, S. A.; Xia, Y. Self-Assembly, Molecular Packing, and Electron Transport in N-Type Polymer Semiconductor Nanobelts. *Chem. Mater.* **2008**, *20* (14), 4712−4719.
(84) Niles, E. T.; Roehling, J. D.; Yamagata, H.; Wise, A. J.; Spano, F. C.; Moulé, A. J.; Grey, J. K. J-Aggregate Behavior in Poly-3-hexylthiophene Nanofibers. *J. Phys. Chem. Lett.* **2012**, *3* (2), 259−263.
(85) Helgesen, M.; Søndergaard, R.; Krebs, F. C. Advanced Materials and Processes for Polymer Solar Cell Devices. *J. Mater. Chem.* **2010**, *20* (1), 36−60.
(86) Dante, M.; Yang, C.; Walker, B.; Wudl, F.; Nguyen, T. Q. Self-Assembly and Charge-Transport Properties of a Polythiophene-Fullerene Triblock Copolymer. *Adv. Mater.* **2010**, *22* (16), 1835−1839.
(87) Yu, J.; Hu, D.; Barbara, P. F. Unmasking Electronic Energy Transfer of Conjugated Polymers by Suppression of O_2 Quenching. *Science* **2000**, *289* (5483), 1327−1330.
(88) Lammi, R. K.; Fritz, K. P.; Scholes, G. D.; Barbara, P. F. Ordering of Single Conjugated Polymers in a Nematic Liquid Crystal Host. *J. Phys. Chem. B* **2004**, *108* (15), 4593−4596.
(89) Schindler, F.; Jacob, J.; Grimsdale, A. C.; Scherf, U.; Müllen, K.; Lupton, J. M.; Feldmann, J. Counting Chromophores in Conjugated Polymers. *Angew. Chem.* **2005**, *117* (10), 1544−1549.
(90) Hildner, R.; Winterling, L.; Lemmer, U.; Scherf, U.; Köhler, J. Single-Molecule Spectroscopy on a Ladder-Type Conjugated Polymer: Electron-Phonon Coupling and Spectral Diffusion. *ChemPhysChem* **2009**, *10* (14), 2524−2534.
(91) Traub, M. C.; Lakhwani, G.; Bolinger, J. C.; Vanden Bout, D. A.; Barbara, P. F. Electronic Energy Transfer in Highly Aligned MEH-PPV Single Chains. *J. Phys. Chem. B* **2011**, *115* (33), 9941−9947.
(92) Tian, Z.; Yu, J.; Wang, X.; Groff, L. C.; Grimland, J. L.; McNeill, J. D. Conjugated Polymer Nanoparticles Incorporating Antifade Additives for Improved Brightness and Photostability. *J. Phys. Chem. B* **2013**, *117* (16), 4517−4520.
(93) Ozel, I. O.; Ozel, T.; Demir, H. V.; Tuncel, D. Non-Radiative Resonance Energy Transfer in Bi-Polymer Nanoparticles of Fluorescent Conjugated Polymers. *Opt. Express* **2010**, *18* (2), 670−684.
(94) Park, E.-J.; Erdem, T.; Ibrahimova, V.; Nizamoglu, S.; Demir, H. V.; Tuncel, D. White-Emitting Conjugated Polymer Nanoparticles with Cross-Linked Shell for Mechanical Stability and Controllable Photometric Properties in Color-Conversion LED Applications. *ACS Nano* **2011**, *5* (4), 2483−2492.
(95) Wang, X.; Groff, L. C.; McNeill, J. D. Photoactivation and Saturated Emission in Blended Conjugated Polymer Nanoparticles. *Langmuir* **2013**, *29* (45), 13925−13931.
(96) Cornil, J.; Dos Santos, D.; Crispin, X.; Silbey, R.; Bredas, J. Influence of Interchain Interactions on the Absorption and Luminescence of Conjugated Oligomers and Polymers: A Quantum-Chemical Characterization. *J. Am. Chem. Soc.* **1998**, *120* (6), 1289−1299.
(97) Yamagata, H.; Norton, J.; Hontz, E.; Olivier, Y.; Beljonne, D.; Brédas, J.-L.; Silbey, R. J.; Spano, F. The Nature of Singlet Excitons in Oligoacene Molecular Crystals. *J. Chem. Phys.* **2011**, *134* (20), 204703.
(98) Siddiqui, S.; Spano, F. H-and J-Aggregates of Conjugated Polymers and Oligomers: A Theoretical Investigation. *Chem. Phys. Lett.* **1999**, *308* (1), 99−105.
(99) Spano, F. C.; Silva, C. H-and J-Aggregate Behavior in Polymeric Semiconductors. *Annu. Rev. Phys. Chem.* **2014**, *65*, 477−500.
(100) Würthner, F.; Kaiser, T. E.; Saha-Möller, C. R. J-Aggregates: From Serendipitous Discovery to Supramolecular Engineering of Functional Dye Materials. *Angew. Chem., Int. Ed.* **2011**, *50* (15), 3376−3410.
(101) Davydov, A. S. The Theory of Molecular Excitons. *Sov. Phys. Usp.* **1964**, *7* (2), 145.
(102) Schlosser, D. W.; Philpott, M. R. Singlet Excitons in Crystalline Naphthalene, Antracene, Tetracene and Pentacene. *Chem. Phys.* **1980**, *49* (2), 181−199.
(103) Yamagata, H.; Hestand, N. J.; Spano, F. C.; Köhler, A.; Scharsich, C.; Hoffmann, S. T.; Bässler, H. The Red-Phase of Poly[2-methoxy-5-(2-ethylhexyloxy)-1,4-phenylenevinylene](MEH-PPV): A Disordered HJ-Aggregate. *J. Chem. Phys.* **2013**, *139* (11), 114903.
(104) Cheng, Y.-C.; Fleming, G. R. Dynamics of Light Harvesting in Photosynthesis. *Annu. Rev. Phys. Chem.* **2009**, *60*, 60.
(105) Atkins, P. W.; Friedman, R. S. *Molecular Quantum Mechanics*; Oxford University Press: 2011.
(106) Capek, V.; Silinsh, E. *Organic Molecular Crystals: Interaction, Localization, and Transport Phenomena*; AIP: New York, 1994.
(107) Pope, M.; Swenberg, C. E. *Electronic Processes in Organic Crystals and Polymers*; Oxford University Press on Demand: 1999.
(108) Renger, T.; May, V.; Kühn, O. Ultrafast Excitation Energy Transfer Dynamics in Photosynthetic Pigment-Protein Complexes. *Phys. Rep.* **2001**, *343* (3), 137−254.
(109) Yang, M.; Fleming, G. R. Influence of Phonons on Exciton Transfer Dynamics: Comparison of the Redfield, Förster, and Modified Redfield Equations. *Chem. Phys.* **2002**, *275* (1), 355−372.
(110) Spano, F. C. The Fundamental Photophysics of Conjugated Oligomer Herringbone Aggregates. *J. Chem. Phys.* **2003**, *118* (2), 981−994.
(111) Spano, F. C. Absorption in Regio-Regular Poly(3-hexyl)-thiophene Thin Films: Fermi Resonances, Interband Coupling and Disorder. *Chem. Phys.* **2006**, *325* (1), 22−35.
(112) Dirac, P. A. The Quantum Theory of the Emission and Absorption of Radiation. *Proc. R. Soc. London, Ser. A* **1927**, *114* (767), 243−265.
(113) Förster, T. Zwischenmolekulare Energiewanderung Und Fluoreszenz. *Ann. Phys.* **1948**, *437* (1−2), 55−75.
(114) Amaldi, E.; Fermi, E. On the Absorption and the Diffusion of Slow Neutrons. *Phys. Rev.* **1936**, *50* (10), 899.
(115) Forrest, S. R. The Path to Ubiquitous and Low-Cost Organic Electronic Appliances on Plastic. *Nature* **2004**, *428* (6986), 911−918.
(116) McNeill, J. D.; O'Connor, D. B.; Barbara, P. F. Imaging Organic Device Function with Near-Field Scanning Optical Microscopy. *J. Chem. Phys.* **2000**, *112* (18), 7811−7821.
(117) Barbara, P.; Adams, D.; O'Connor, D. Characterization of Organic Thin Film Materials with Near-Field Scanning Optical Microscopy (NSOM). *Annu. Rev. Mater. Sci.* **1999**, *29* (1), 433−469.
(118) Lakowicz, J. R. *Principles of Fluorescence Spectroscopy*; Springer Science & Business Media: 2013.
(119) Tapping, P. C.; Clafton, S. N.; Schwarz, K. N.; Kee, T. W.; Huang, D. M. Molecular-Level Details of Morphology-Dependent Exciton Migration in Poly(3-hexylthiophene) Nanostructures. *J. Phys. Chem. C* **2015**, *119* (13), 7047−7059.
(120) Crank, J. *The Mathematics of Diffusion*. Oxford university press: 1979.
(121) Fan, C.; Wang, S.; Hong, J. W.; Bazan, G. C.; Plaxco, K. W.; Heeger, A. J. Beyond Superquenching: Hyper-Efficient Energy Transfer from Conjugated Polymers to Gold Nanoparticles. *Proc. Natl. Acad. Sci. U. S. A.* **2003**, *100* (11), 6297−6301.
(122) Gösele, U.; Hauser, M.; Klein, U.; Frey, R. Diffusion and Long-Range Energy Transfer. *Chem. Phys. Lett.* **1975**, *34* (3), 519−522.
(123) Powell, R. C. Host-Sensitized Energy Transfer in Molecular Crystals. *Phys. Rev. B* **1970**, *2* (4), 1159.
(124) Hsu, C.; Powell, R. C. Energy Transfer in Europium Doped Yttrium Vanadate Crystals. *J. Lumin.* **1975**, *10* (5), 273−293.
(125) Yip, W.-T.; Hu, D.; Yu, J.; Vanden Bout, D. A.; Barbara, P. F. Classifying the Photophysical Dynamics of Single-and Multiple-Chromophoric Molecules by Single Molecule Spectroscopy. *J. Phys. Chem. A* **1998**, *102* (39), 7564−7575.
(126) Yu, J.; Lammi, R.; Gesquiere, A. J.; Barbara, P. F. Singlet-Triplet and Triplet-Triplet Interactions in Conjugated Polymer Single Molecules. *J. Phys. Chem. B* **2005**, *109* (20), 10025−10034.
(127) Vanden Bout, D. A.; Yip, W.-T.; Hu, D.; Fu, D.-K.; Swager, T. M.; Barbara, P. F. Discrete Intensity Jumps and Intramolecular Electronic Energy Transfer in the Spectroscopy of Single Conjugated Polymer Molecules. *Science* **1997**, *277* (5329), 1074−1077.
(128) Barth, S.; Bässler, H.; Wehrmeister, T.; Müllen, K. Photoconduction in Oligo-Para-Phenylenevinylene Films. *J. Chem. Phys.* **1997**, *106* (1), 321−327.

DOI: 10.1021/acs.chemrev.6b00419
Chem. Rev. XXXX, XXX, XXX−XXX

(129) McNeill, J. D.; Barbara, P. F. Nsom Investigation of Carrier Generation, Recombination, and Drift in a Conjugated Polymer. *J. Phys. Chem. B* **2002**, *106* (18), 4632−4639.
(130) McNeill, J. D.; O'Connor, D. B.; Adams, D. M.; Barbara, P. F.; Kämmer, S. B. Field-Induced Photoluminescence Modulation of MEH-PPV under Near-Field Optical Excitation. *J. Phys. Chem. B* **2001**, *105* (1), 76−82.
(131) Williams, G.; Watts, D. C. Non-Symmetrical Dielectric Relaxation Behaviour Arising from a Simple Empirical Decay Function. *Trans. Faraday Soc.* **1970**, *66*, 80−85.
(132) Bakulin, A. A.; Lovrincic, R.; Yu, X.; Selig, O.; Bakker, H. J.; Rezus, Y. L.; Nayak, P. K.; Fonari, A.; Coropceanu, V.; Brédas, J.-L. Mode-Selective Vibrational Modulation of Charge Transport in Organic Electronic Devices. *Nat. Commun.* **2015**, *6*, 7880.
(133) Clafton, S. N.; Huang, D. M.; Massey, W. R.; Kee, T. W. Femtosecond Dynamics of Excitons and Hole-Polarons in Composite P3HT/PCBM Nanoparticles. *J. Phys. Chem. B* **2013**, *117* (16), 4626−4633.
(134) Clafton, S. N.; Beattie, D. A.; Mierczynska-Vasilev, A.; Acres, R. G.; Morgan, A. C.; Kee, T. W. Chemical Defects in the Highly Fluorescent Conjugated Polymer Dots. *Langmuir* **2010**, *26* (23), 17785−17789.
(135) Plakhotnik, T.; Donley, E. A.; Wild, U. P. Single-Molecule Spectroscopy. *Annu. Rev. Phys. Chem.* **1997**, *48* (1), 181−212.
(136) Thompson, R. E.; Larson, D. R.; Webb, W. W. Precise Nanometer Localization Analysis for Individual Fluorescent Probes. *Biophys. J.* **2002**, *82* (5), 2775−2783.
(137) Blom, P.; De Jong, M.; Vleggaar, J. Electron and Hole Transport in Poly(p-phenylene vinylene) Devices. *Appl. Phys. Lett.* **1996**, *68* (23), 3308−3310.
(138) Bozano, L.; Carter, S.; Scott, J.; Malliaras, G.; Brock, P. Temperature-and Field-Dependent Electron and Hole Mobilities in Polymer Light-Emitting Diodes. *Appl. Phys. Lett.* **1999**, *74* (8), 1132.
(139) Bässler, H.; Köhler, A. Charge Transport in Organic Semiconductors. *Top. Curr. Chem.* **2011**, *312*, 1−66.
(140) Fishchuk, I.; Arkhipov, V.; Kadashchuk, A.; Heremans, P.; Bässler, H. Analytic Model of Hopping Mobility at Large Charge Carrier Concentrations in Disordered Organic Semiconductors: Polarons Versus Bare Charge Carriers. *Phys. Rev. B: Condens. Matter Mater. Phys.* **2007**, *76* (4), 045210.
(141) Yamagata, H.; Spano, F. C. Interplay between Intrachain and Interchain Interactions in Semiconducting Polymer Assemblies: The HJ-Aggregate Model. *J. Chem. Phys.* **2012**, *136* (18), 184901.

DOI: 10.1021/acs.chemrev.6b00419
Chem. Rev. XXXX, XXX, XXX−XXX